

AD-A055 195

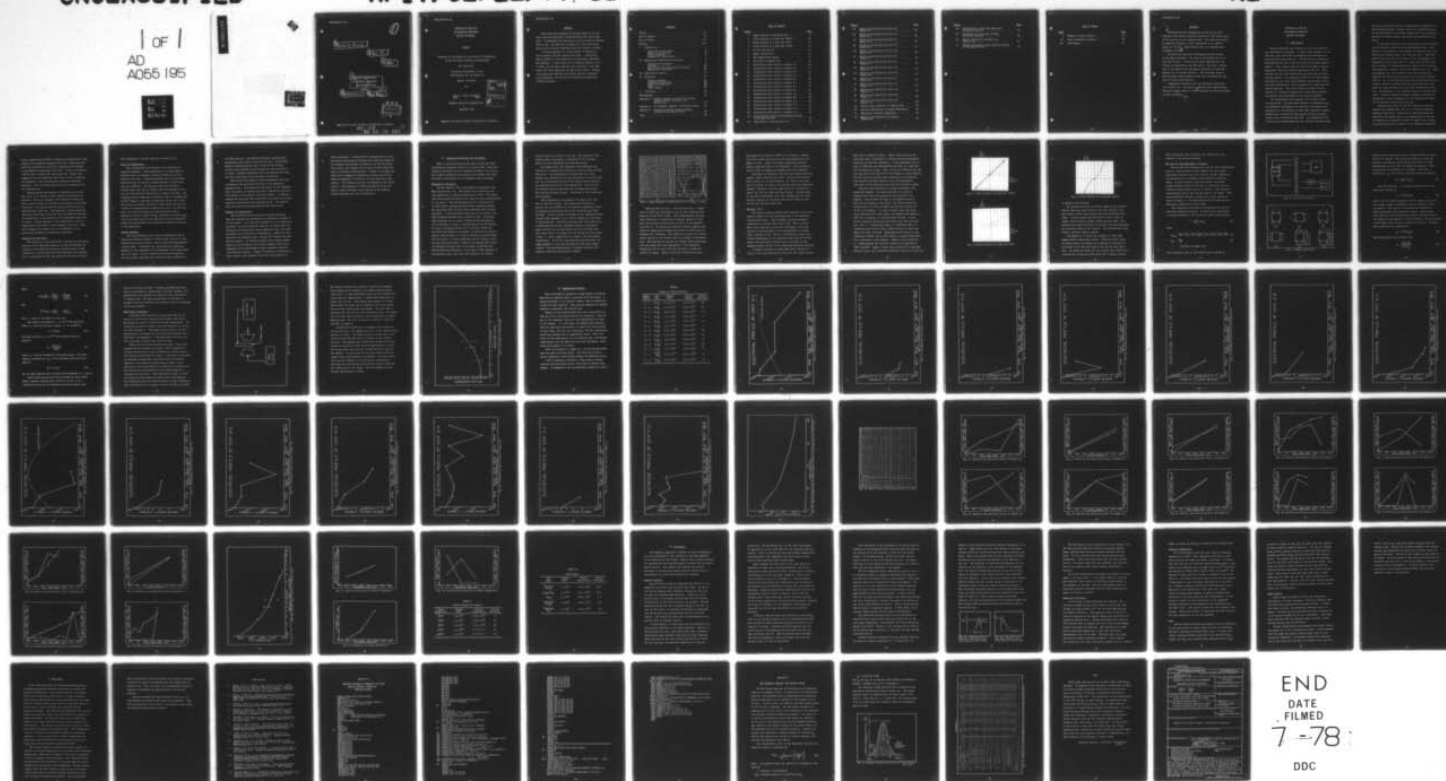
AIR FORCE INST OF TECH WRIGHT-PATTERSON AFB OHIO SCH--ETC F/G 20/12
ELECTRICAL PROFILING OF MAGNESIUM IMPLANTED GALLIUM PHOSPHIDE.(U)
DEC 77 D J LANK

UNCLASSIFIED

AFIT/GE/EE/77-38

NL

1 of 1
AD
A055 195



1

9 Master's thesis,

11 Dec 77

12 88 p.

6
ELECTRICAL PROFILING
OF MAGNESIUM IMPLANTED
GALLIUM PHOSPHIDE .

THESIS

14 AFIT/GE/EE/77-38

10 David Lank
Capt USAF

James

DDC
RECEIVED
JUN 19 1978
E

Approved for public release; distribution unlimited.

022 225

78 06 13 160

sk

ELECTRICAL PROFILING
OF MAGNESIUM IMPLANTED
GALLIUM PHOSPHIDE

THESIS

Presented to the Faculty of the School of Engineering
of the Air Force Institute of Technology

Air University

in Partial Fulfillment of the
Requirements for the Degree of

Master of Science

by

David J. Lank, B.S.E&C.E.
Capt USAF

Graduate Electrical Engineering

December 1977

ACCESSION for	
NTIS	White Section <input checked="" type="checkbox"/>
DDC	Buff Section <input type="checkbox"/>
UNANNOUNCED	<input type="checkbox"/>
JUSTIFICATION.....	
BY.....	
DISTRIBUTION/AVAILABILITY CODES	
Dist.	AVAIL. and/or SPECIAL
A	

Preface

This study was sponsored by the DHR branch of the Air Force Avionics Laboratory, Wright-Patterson Air Force Base, Ohio. It developed from the need to know how various implants work in GaP. The work was in support of other work being done at the Air Force laboratory and with outside contracts.

I am very grateful to a great number of people for their guidance and help during this study. I especially want to thank Dr. Bill Dobbs for his invaluable assistance and guidance. I also would like to thank my sponsor, Dr. Y. S. Park, and Jim Ehret and the other personnel of the DHR branch for their assistance during my work there. Finally, I am especially indebted to my thesis advisor, Professor Jerzy Lubelfeld, for his own way of making my experience at AFIT tolerable.

Contents

Preface	ii
List of Figures	iv
List of Tables	vii
Abstract	viii
I. Introduction	1
Objective of this Study	3
Scope and Assumptions	4
General Approach	4
Sequence of Presentation	5
II. Experimental Methods and Processing	7
Preparatory Procedures	7
Contacts	10
The van der Pauw Measurement Procedure	14
Measurement Procedures	18
III. Experimental Results	22
IV. Discussion	51
Density Profiles	51
Conversion Efficiency	55
Annealing Temperature	56
Caps	56
Other Results	57
V. Conclusion	59
Bibliography	61
Appendix A: Computer Program to Calculate and Plot Carrier Density, Mobility, and Resistivity	62
Appendix B: The Lindhard, Scharff, and Schiott Theory	66
Appendix C: Gibbons and Johnson Range Estimates Listing for Mg Implanted GaP	68
Vita	69

List of Figures

<u>Figure</u>		<u>Page</u>
1	Auger Analysis of Sputtered Caps	9
2	Au/Zn Contacts on p-type GaP (296°K)	12
3	Au/Zn Contacts on p-type GaP (96°K)	12
4	Au/Zn Contacts on n-type GaP (296°K)	13
5	van der Pauw Set-up	15
6	Sample Connections	15
7	Hall Measurement System	19
8	Etch Rate vs Implant Dose	21
9	Differential Hall Profile of Sample S-1 . .	24
10	Differential Hall Profile of Sample S-2 . .	25
11	Differential Hall Profile of Sample S-3 . .	26
12	Differential Hall Profile of Sample S-4 . .	27
13	Differential Hall Profile of Sample S-5 . .	28
14	Differential Hall Profile of Sample S-6 . .	29
15	Differential Hall Profile of Sample E-1 . .	30
16	Differential Hall Profile of Sample E-3 . .	31
17	Differential Hall Profile of Sample E-4 . .	32
18	Differential Hall Profile of Sample N-2 . .	33
19	Differential Hall Profile of Sample N-3 . .	34
20	Differential Hall Profile of Sample N-4 . .	35
21	Differential Hall Profile of Sample C-1 . .	36
22	Differential Hall Profile of Sample C-3 . .	37
23	Glow Discharge Optical Spectrography Profile of Mg Implanted GaP	38
24	GDOS Profile of Mg Implanted GaP	39

<u>Figure</u>		<u>Page</u>
25	Mobility and Resistivity Plots for Sample S-1	40
26	Mobility and Resistivity Plots for Sample S-2	40
27	Mobility and Resistivity Plots for Sample S-3	41
28	Mobility and Resistivity Plots for Sample S-4	41
29	Mobility and Resistivity Plots for Sample S-5	42
30	Mobility and Resistivity Plots for Sample S-6	42
31	Mobility and Resistivity Plots for Sample E-1	43
32	Mobility and Resistivity Plots for Sample E-3	43
33	Mobility and Resistivity Plots for Sample E-4	44
34	Mobility and Resistivity Plots for Sample N-2	44
35	Mobility and Resistivity Plots for Sample N-3	45
36	Mobility and Resistivity Plots for Sample N-4	45
37	Mobility and Resistivity Plots for Sample C-1	46
38	Mobility and Resistivity Plots for Sample C-3	46
39	Percent Type Conversion vs Implant Dose . .	47
40	Carrier Concentration vs Anneal Temperature	48
41	Efficiency vs Anneal Temperature	48
42	Mobility and Resistivity vs Anneal Temperature	49

<u>Figure</u>		<u>Page</u>
43	Distribution of Ions when Electronic Collisions Dominate	54
44	Distribution of Ions when Nuclear Collisions Dominate	54
B1	Typical Theoretical Gaussian Ion Distribution	67
C1	Gibbons and Johnson Range Estimate Listing for Mg Implanted GaP	68

List of Tables

<u>Table</u>		<u>Page</u>
I	Summary of Chips Profiled	23
II	Anneal Temperature Summary	49
III	Caps Summary	50

Abstract

Differential Hall measurements by the van der Pauw technique were taken to provide a profile of the electrically active carriers in ion implanted GaP. The study was limited to magnesium implants at room temperature at an implant energy of 129 KeV. Annealing was done in a flowing argon atmosphere at 900°C.

The profiles indicated a decreasing carrier density as the depth increased. The peak of the profile was at or near the surface. In none of the cases observed were the results as predicted by the LSS theory. They were, however, much in accordance with the theory developed by Large and Bicknel for low energy implants. Glow Discharge Optical Spectrography (GDOS) profiles taken also indicated the same type of carrier distribution.

Temperature dependence and cap dependence tests were also carried out. The results indicated that pyrolytically deposited Si_3N_4 annealed at 900°C provided the best percentage of type conversion.

ELECTRICAL PROFILING
OF MAGNESIUM IMPLANTED
GALLIUM PHOSPHIDE

I. Introduction

Gallium phosphide has recently received new attention as a semiconductor material. It has a wider bandgap, 2.8 eV, than most other semiconductor materials and therefore has many potential uses (Ref 2:7). The Air Force is presently investigating the use of GaP for satellite attitude sensors (Ref 9). Other current uses for GaP include FET's, optical waveguides, and solar assisted hydrolysis (Ref 10). This material has been used extensively for green and red light emitting diodes. One advantage related to its wide bandgap that GaP has over other semiconductors such as GaAs is the fact that GaP produces, and is sensitive to, light over the visible spectrum. Much of the growth potential of this material is presently untapped due to processing problems and because the raw material is not easily available.

Ion implantation would appear to be an ideal method for doping GaP. The high vapor pressure of phosphorus and the subsequent breakdown of the material into gallium and phosphorus at low temperatures make high temperature doping methods such as diffusion from gaseous sources and doped oxides a poor alternative (Ref 2:8). Ion implantation can be done at room temperature and the required annealing steps

are short and relatively low in temperature in comparison to other doping methods. However, before ion implantation can be used effectively as a means of doping GaP, the electrical activity of various dopant ions within the material must be known.

It has been shown that both p-type and n-type conversion can be achieved in GaP using various implanted ions. The percent of conversion, or the percent of implanted ions that become electrically active, has been quite low. Inada and Ohnuki have done work in the area of zinc and magnesium ion implantation previously (Ref 6). Other work has also been done by Gelpey at the Massachusetts Institute of Technology with magnesium, selenium, and sulfur implants (Ref 2). Dobbs and Hemenger have also worked in the area studying zinc implants and Dobbs has also worked with beryllium implants (Ref 5). All of this previous work has demonstrated and the current work has confirmed that type conversion does take place but that the percent of this type conversion is very low. For magnesium, it is normally around ten percent (Ref 2:10). Until an effective method is found to increase the percentage of type conversion, the ion implantation method is not meeting its potential with GaP.

From previous work, it has been discovered that ion implantation damages GaP, that is, it turns the material amorphous (Ref 2:10). Work done by Inada and Ohnuki has shown that the damage done by ion implantation is removed by annealing the material at 800°C or higher, but in order to achieve electrical activity of the implanted impurities,

anneal temperatures of 900°C or higher are needed (Ref 7:229). Gelpey's work slightly disagreed with this, indicating that 850°C was sufficient to activate a significant percentage of the magnesium impurities (Ref 2:74). He did not, however, indicate what a significant percentage was. Gelpey also suggested that the implanted impurities, as well as gallium and phosphorus, were diffusing out during the annealing procedure. Silicon dioxide was used as the encapsulant for his investigation.

Several groups have studied ion implantation in GaAs and, since it is similar to GaP, similar results might be expected. There are, however, some important differences. Since neither oxides nor nitrides can be grown on these semiconductors, caps used during the annealing process must be deposited some other way. The adherence of these deposited coatings is much weaker with GaP than with GaAs and therefore the probability of out-diffusion of the implanted impurities is higher. Another problem is the decomposition of GaP at temperatures above 600°C at one atmosphere (Ref 2:8). This also increases the probability of out-diffusion of the gallium and phosphorus as previously mentioned.

Objective of this Study

The objective of this study was to profile the electrical activity of ion implanted magnesium in GaP to determine the location of the implanted layer and the percentage of type conversion or electrically activated magnesium ions obtained; also, to determine why low type conversion has been obtained

with magnesium in the past and how to correct for it.

Scope and Assumptions

This investigation was limited to the profiling of magnesium implants. Since magnesium is a p-type dopant if substitutional for gallium, contacts designed for p-type material were used. Contacting methods had to be developed that would work on GaP since normal methods of contacting were not effective. The implant energy was limited to 129 KeV since this was the highest that was obtainable with the Air Force Avionics Laboratory ion implant facility. All annealing except temperature dependence runs was accomplished at 900°C based on work done by Inada and Ohnuki (Ref 7:229). The Lindhard, Scharff, and Schiott (LSS) theory was used as a basis for determining etch depths and rates. For the most part, the caps used during the annealing process were limited to silicon nitride (Si_3N_4) and silicon dioxide (SiO_2) since these were the only two caps which could be deposited using both the pyrolytic and sputtering techniques available in the laboratory.

General Approach

The first necessary step of this investigation was to develop an effective method of forming ohmic contacts to the GaP substrate because without them no electrical measurements could be made. A suitable cap, used during the annealing process for the prevention of out-diffusion of the impurities, had to be found. Silicon nitride and silicon dioxide were the two primary caps used since these two were available in

the AFAL facility. Two different methods, pyrolytic and sputtering, were tried to find the best one. An effective method of determining the rate of etch of the etching solution and a method of controlling the rate also had to be found. Standard procedures with some modifications were used for other steps in the process of profiling.

The van der Pauw method of Hall measurements was used to determine the electrical activity of the implanted magnesium ions. By etching off thin layers of the implanted GaP, the profile of electrically active impurities was made with respect to the distance from the surface. A computer program was developed that calculated and plotted the profile from data obtained from the experimentation. The program also calculated and plotted mobility and resistivity.

Sequence of Presentation

The experimental methods and processing techniques that were employed and developed are contained in Chapter II of this thesis. It covers the development of the contacting procedure, the method used for capping, the method used for profiling the electrically active magnesium ions, and other procedures used during this investigation. Chapter II also describes the equipment used. Chapter III contains the data and the results. It includes graphical and tabular presentation of the profiles of the various samples tested and a comparison of the percentage of type conversion obtained with different samples. Chapter IV presents a discussion of these results and interprets them from the standpoint of

their importance. It presents two explanations as to why decreasing concentration profiles were obtained instead of the Gaussian distribution as predicted by the LSS theory. This chapter also compares the results of this study with those of previous investigations. Chapter V concludes the study with a summary of significant results such as the higher percentage of conversion obtained than with other studies. This chapter also has recommendations for future studies. The appendices include information on the LSS theory, range estimates, and a listing of the computer program developed for this investigation.

II. Experimental Methods and Processing

Many of the processing methods used on GaAs and other semiconductor materials could not be used on GaP. Even some standard procedures had to be modified somewhat for use here. This chapter presents the procedures used during this study and gives a description of the equipment where necessary.

Preparatory Procedures

The GaP used for this investigation was obtained from Metal Specialties, Inc. The material was received as two inch wafers with a crystal orientation of (100). The wafers were then scribed and broken into chips that were approximately 0.5 cm square. This was determined to be a suitable size to work without causing any significant handling problems. The chips were then cleaned using a modified GaAs cleaning procedure. It was discovered that many of the steps in the GaAs cleaning procedure had no effect on GaP. The method used consisted of: 1) rinse in flowing trichloroethylene for 20 seconds, 2) rinse in flowing acetone for 20 seconds, 3) rinse in flowing methanol for 20 seconds, 4) blow dry with inert gas (argon or nitrogen), 5) wash with 10 percent aquasol soap solution, 6) rinse in flowing de-ionized water for one minute, 7) rinse in methanol for 20 seconds, and 8) blow dry using inert gas. Steps in the GaAs procedure such as etching in HF had little or no effect on GaP and were deleted from the procedure. In the case of four samples, to be described later, the chips were etched in an etching

solution which was found to etch GaP. The chips were then checked under a microscope to determine if all foreign matter had been removed by the cleaning process.

The samples were then implanted with magnesium ions using the ion implantation facility in the Air Force Avionics Laboratory. The Accelerators, Incorporated unit could produce only 129 KeV but this was determined to be sufficient for this investigation based on LSS theory range estimates. All implants were done at room temperature. Both hot and cold cathode sources were used for the magnesium sources and both gave similar results. The source in both cases was pure magnesium.

After implanting, the samples were capped with from 1000 to 2000 Å of Si_3N_4 . The capping was necessary to prevent the out-diffusion of the implanted magnesium as well as phosphorus and gallium during the annealing step which followed. Silicon nitride was chosen as the capping material because there appeared to be a better adhesion of the layer to the substrate. Both SiO_2 and Si_3N_4 were tried using both a sputtering method and a pyrolytic method of deposition. Auger analysis of the caps showed that the sputtered caps had a high content of oxygen near the surface as can be seen in Fig. 1. Since oxygen acts as a dopant, this was highly undesirable. Of the two caps deposited pyrolytically, the Si_3N_4 appeared to have the best adhesion and least oxygen content. The sputtering methods in general had much less adherence than did the pyrolytic methods.

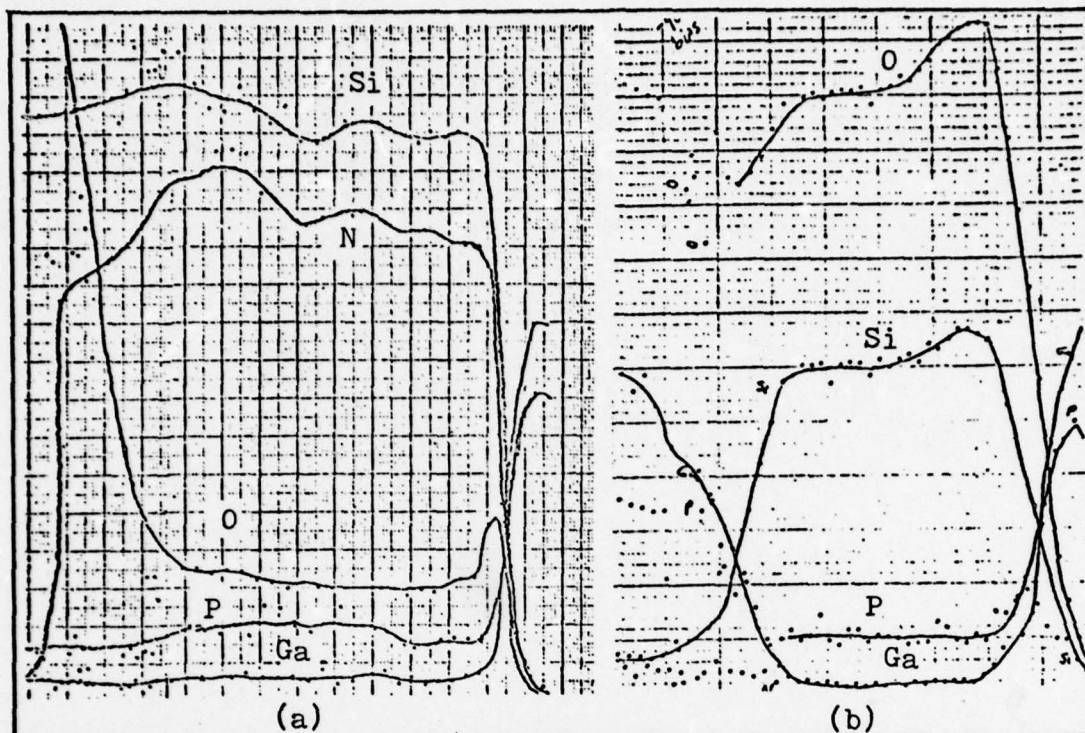


Fig. 1. Auger Analysis of Sputtered Caps: a) Si_3N_4 , b) SiO_2

Annealing was done next. From previous work, a temperature of 900°C was determined to be the best annealing temperature for GaP (Ref 7:229). Lower temperatures have been found effective in correcting the implant damage but they have not produced substitutional activity of the implanted ions (Ref 7). To verify this previous finding, samples were tested at temperatures ranging from 800°C to 1000°C and the findings were confirmed. The samples were placed in a glass holder and put in the furnace tube but outside of the heated area. This was done to prevent the thermal shock associated with the change from room temperature to the annealing temperature and to allow time for the argon to purge the furnace of oxygen. After a ten minute transition period,

the samples were heated at 900°C for 30 minutes. Another ten minute period was allowed after the annealing for the sample to cool. During the entire annealing procedure, flowing argon was used as the atmosphere. This provided a clean as well as oxygen and nitrogen free dry atmosphere.

Following the annealing, the caps were removed from the samples using a 48% solution of HF. Since the HF solution had no effect on the GaP substrate, the time of this etch was not critical so long as the nitride layer was completely removed. Normally, the time used was 20 to 40 minutes to ensure that all the layer had been removed. In some cases it was hard to determine from color changes when the layer had been removed, so the extra time was an insurance that all the cap had been etched off.

Contacts (Ref 1)

The normal method of making ohmic contacts to most substrates consists of just soldering leads to the substrate using indium solder. This procedure provided extremely unsatisfactory results when used on GaP. Those contacts which were conductive at all were rectifying. Much work was done at the beginning of this investigation on making ohmic contacts to GaP. Since it was desired to make electrical measurements of the implanted layer and not the substrate, the electrical contacts had to be ohmic to the implanted layer but not to the underlying substrate material.

A number of metals or alloys make ohmic contacts on both p- and n-type material but they will not ensure contact

with only the implanted layer. Ohmic contact to only the implanted layer is necessary to obtain accurate measurements using the van der Pauw technique. It was determined that an alloy of 88% gold and 12% germanium was ohmic on n-type GaP but rectifying on p-type. Also, an alloy of 85% gold and 15% zinc was ohmic on p-type GaP but rectifying on n-type material. The fact that the contacts were rectifying on the opposite type material provided insurance that the measurements taken were of the implanted layer and not the entire sample.

The alloy was sputtered in an argon atmosphere onto masked GaP samples. The mask consisted of a piece of aluminum foil with holes punched at the corners of the samples. This allowed the alloy to be deposited only at spots at the corners of the chips. The normal sputtering current was 10 to 12 ma at 1200 volts and was carried out for 20 to 30 minutes. To obtain contacts that were ohmic from these deposited alloy areas, the samples were heated to 500°C for 10 minutes in a flowing argon furnace. A five minute transition period was used before and after the heating. The I - V curves were taken on a Tektronix type 575 transistor-curve tracer using a probe station to check each sample for ohmic contacts. Measurements were taken at room temperature (296°K) and at 96°K using a Cryogenic Technology, Inc. cryocooler on test samples. Figures 2 and 3 show the I - V measurements for the Au/Zn contact on p-type GaP at 296°K and 96°K. Figure 4 shows these contacts on n-type GaP. Similar results were obtained using Au/Ge alloy as the contacts

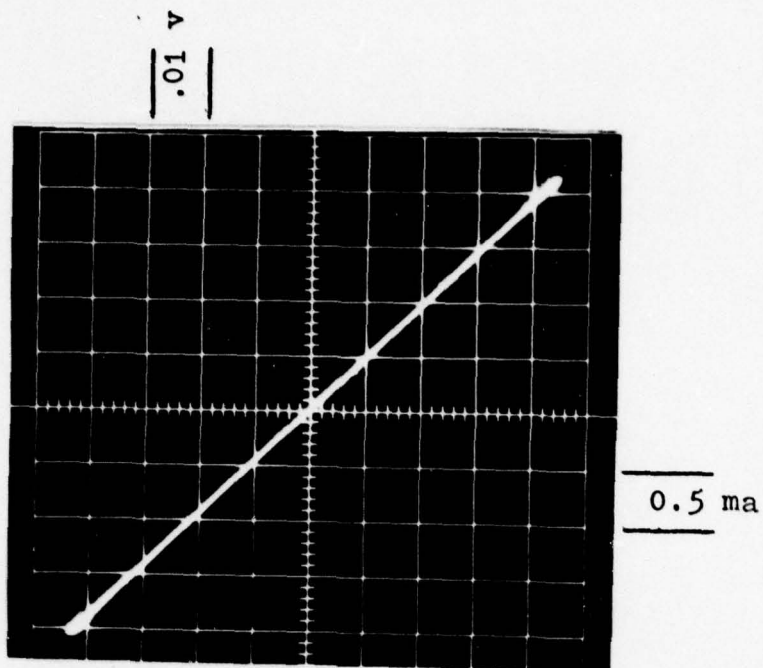


Fig. 2. Au/Zn Contacts on p-type GaP (296°K)

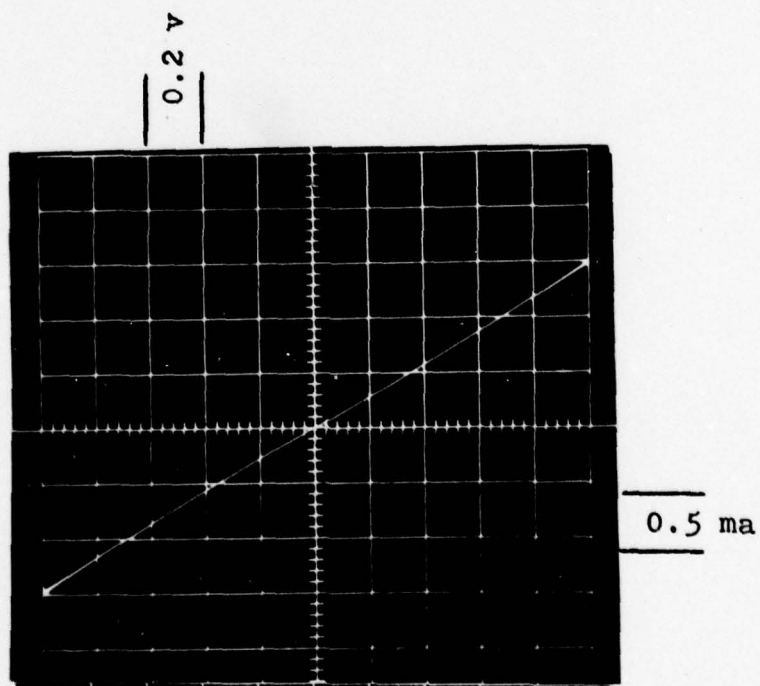


Fig. 3. Au/Zn Contacts on p-type GaP (96°K)

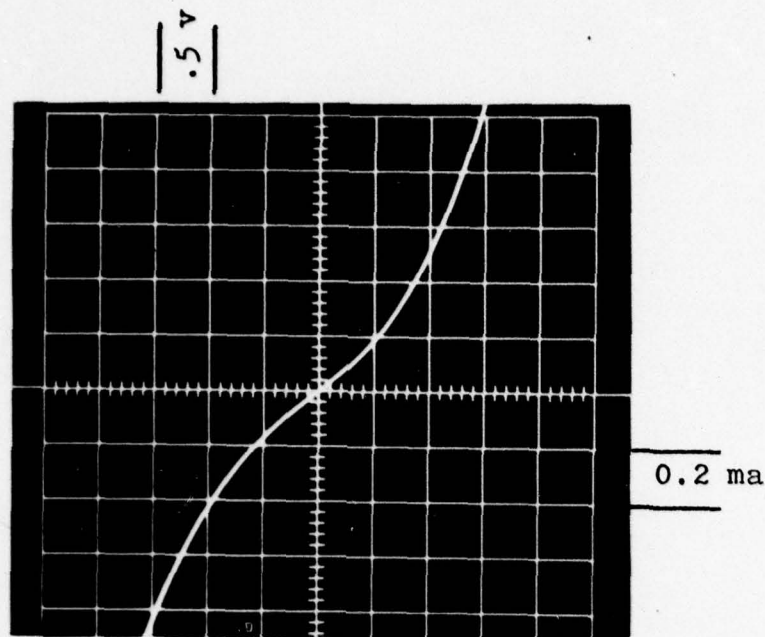


Fig. 4. Au/Zn Contacts on n-type GaP (296°K)

on opposite type material.

Two methods were used to connect leads to the contacts. Indium solder was used but due to the heat involved with this method, leads often became loose when soldering other leads. A silver epoxy made from silver, with a trace of copper, and an acrylic polymer binder was also used. This material was tested and found to provide a very good physical and electrical bond to the contacts. Both methods were used, however, and gave similar results.

The sample to be tested was mounted on a wand type sample holder using rubber cement. Using the silver epoxy or indium solder, the sample was connected electrically to the leads on the wand that lead to the van der Pauw equipment. The epoxy or solder and the contacts were coated with a protective coating of either black wax or krylon lacquer.

This coating was used to protect the contacts from the effects of the repeated etchings.

The van der Pauw Measurement Procedure

The van der Pauw technique was used for this investigation since it could be used on small samples and thin layers. This method required only four contacts located anywhere on the periphery of an uniformly thick sample of arbitrary shape. It was necessary, with this system, to measure across different pairs of contacts to correct for the non-uniform distance between pairs of contacts. This required interchanging current and voltage leads to the sample. This was accomplished through a six-position rotary switch as shown in Figure 5. All measurements could be made without physically changing any of the leads.

The calculations involved in determining the profile used many different formulas. To obtain bulk resistivity, ρ , in ohm-centimeters, the following formula was employed:

$$\rho = \frac{\pi t}{\ln 2} (R_{avg}) \quad (1)$$

where

$$R_{avg} = \frac{R_{a1} + R_{a2} + R_{b1} + R_{b2} + R_{c1} + R_{c2} + R_{d1} + R_{d2}}{8} \quad (2)$$

$$R_{a1} = \frac{V_{a1}}{I} \quad (3)$$

t = thickness of sample (cm)

The resistances used in this formula were obtained by

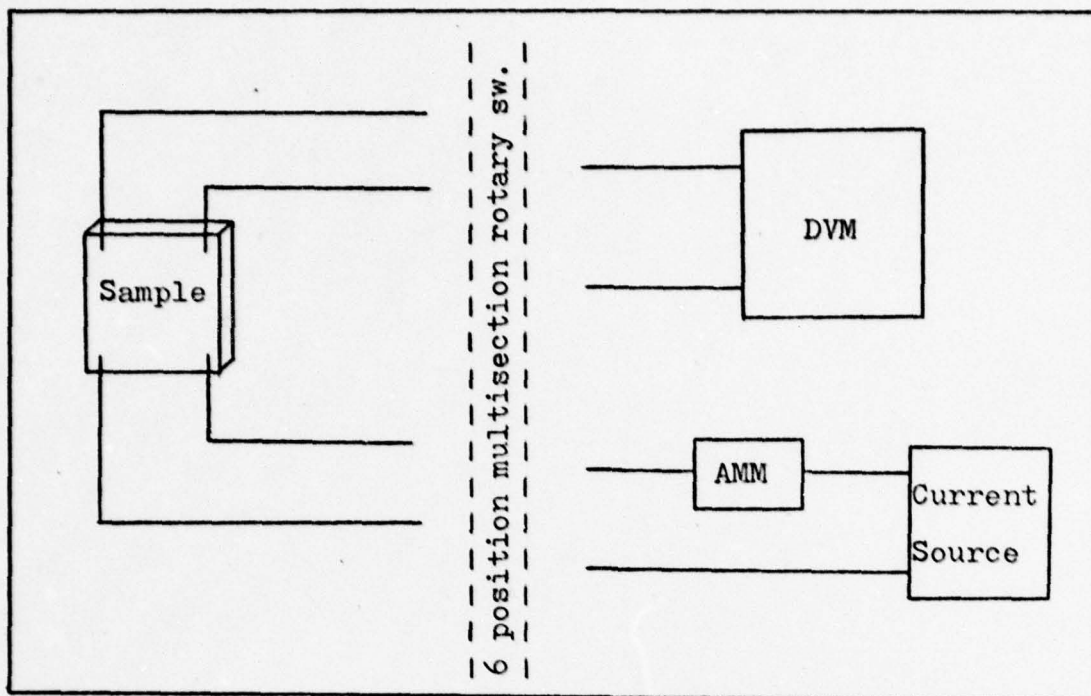


Fig. 5. van der Pauw Set-up

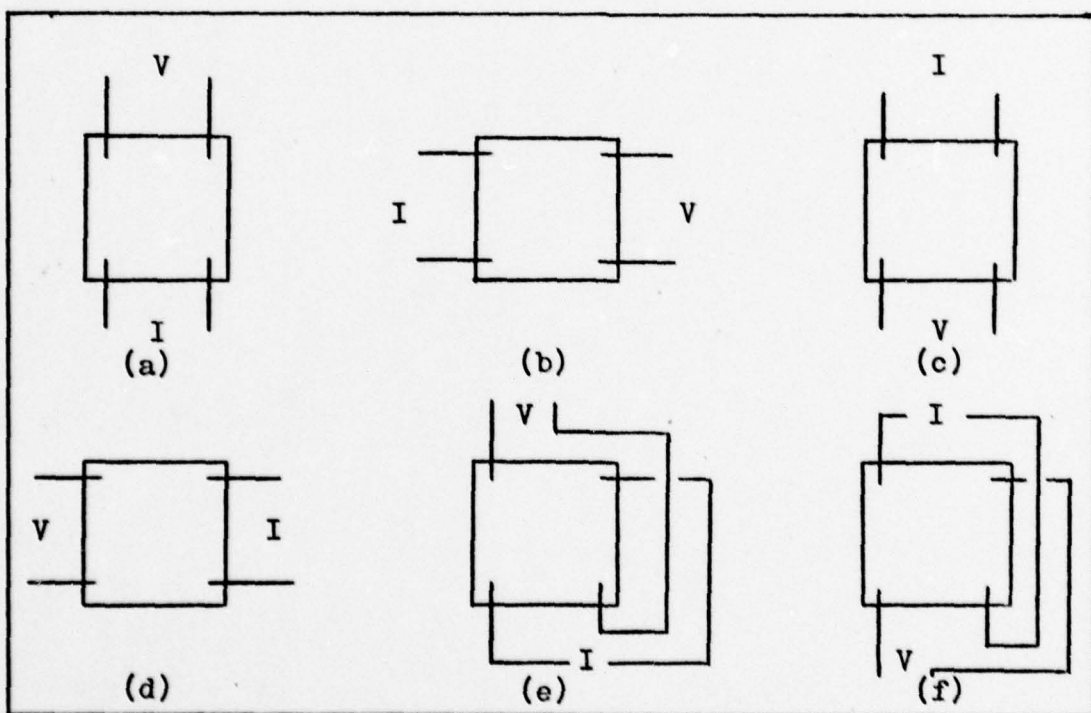


Fig. 6. Sample Connections

measuring the voltage across the V leads as shown in Figure 6a, 6b, 6c, and 6d. The current was applied in both the positive and negative directions giving a total of eight measurements for each time the sample was measured. This corrected for the geometry of the sample. The sheet resistivity, ρ_s , was obtained similarly using the equation

$$\rho_s = \frac{\pi}{\ln 2} (R_{\text{avg}}) \quad (4)$$

The Hall mobility, μ , in square centimeters per volt-second was obtained by

$$\mu = 10^8 (\Delta R_e / B) \quad (5)$$

where B was the applied magnetic field in gauss and ΔR_e was the average change in resistance when the magnetic field was applied. The change in resistance was obtained by eight measurements and averaged as before. Measurements were taken with both positive and negative current and with the magnetic field applied in both directions. The connections to the sample were as shown in Figures 6e and 6f. The sheet Hall coefficient was found using

$$R_s = 10^8 (\Delta R_e / B) \quad (6)$$

The sheet mobility was obtained from

$$\mu_i = \frac{\Delta(R_s / \rho_s^2)_i}{\Delta(1/\rho_s)_i} \quad (7)$$

where

$$\Delta(R_s/\rho_s^2)_i = \frac{(R_s)_i}{(\rho_s)_i^2} - \frac{(R_s)_{i+1}}{(\rho_s)_{i+1}^2} \quad (8)$$

and

$$\Delta(1/\rho_s)_i = \frac{1}{(\rho_s)_i} - \frac{1}{(\rho_s)_{i+1}} \quad (9)$$

with i equal to the number of the etch.

The carrier concentration, n , in cm^{-2} was calculated from ρ , μ , and the electronic charge, e , in coulombs by

$$n = 1/(\rho e \mu) \quad (10)$$

The sheet density, n_i , in cm^{-3} was obtained using the equation

$$n_i = \frac{\Delta(1/\rho_s)_i}{e d_i \mu_i} \quad (11)$$

where d_i was the thickness of the etched layer. The total carrier concentration, N_s , of the implanted layer was determined by

$$N_s = \sum n_i d_i \quad (12)$$

All of these formulas were obtained from References 4, 8, and 12.

Since these calculations had to be made for each etched layer, computer programs were written to do all of the calculations and plot the resultant calculated carrier den-

sity as a function of depth. Computer programs were also used to plot mobility, resistivity, and other results. The programs were also written to output the data and results in tabular form. The main program used is included in Appendix A and the results of the computer runs are contained in the next chapter.

Measurement Procedures

A Keithley Model 225 current source was used as the source of current and a Systron-Donner Model 7205 Digital Multimeter was used to obtain the voltage measurements. The wiring was as shown in Figure 5 and the equipment set-up was as shown in Figure 7. The magnet used produced a field of approximately 7500 gauss and this field was measured with a Bell Model 615 Gaussmeter. A Keithley Model 610C Electrometer was used to monitor the current source.

After each set of measurements were made, a layer was removed from the surface by etching. Since conventional etching methods did not prove satisfactory, another method and etching solution had to be used. A solution of two grams of potassium ferricyanide, six milliliters of potassium hydroxide, and enough de-ionized water to make a total solution of 150 ml was found to be effective in etching GaP. The etching rate was measured for an undoped sample to determine the etch rate. This resulted in a rate of 105 Å per minute for the p-type GaP used in this investigation. All etching was done in a stirred solution using a Thermolyne Type 1000 Stirplate at a speed of either 600 RPM or 300 RPM.

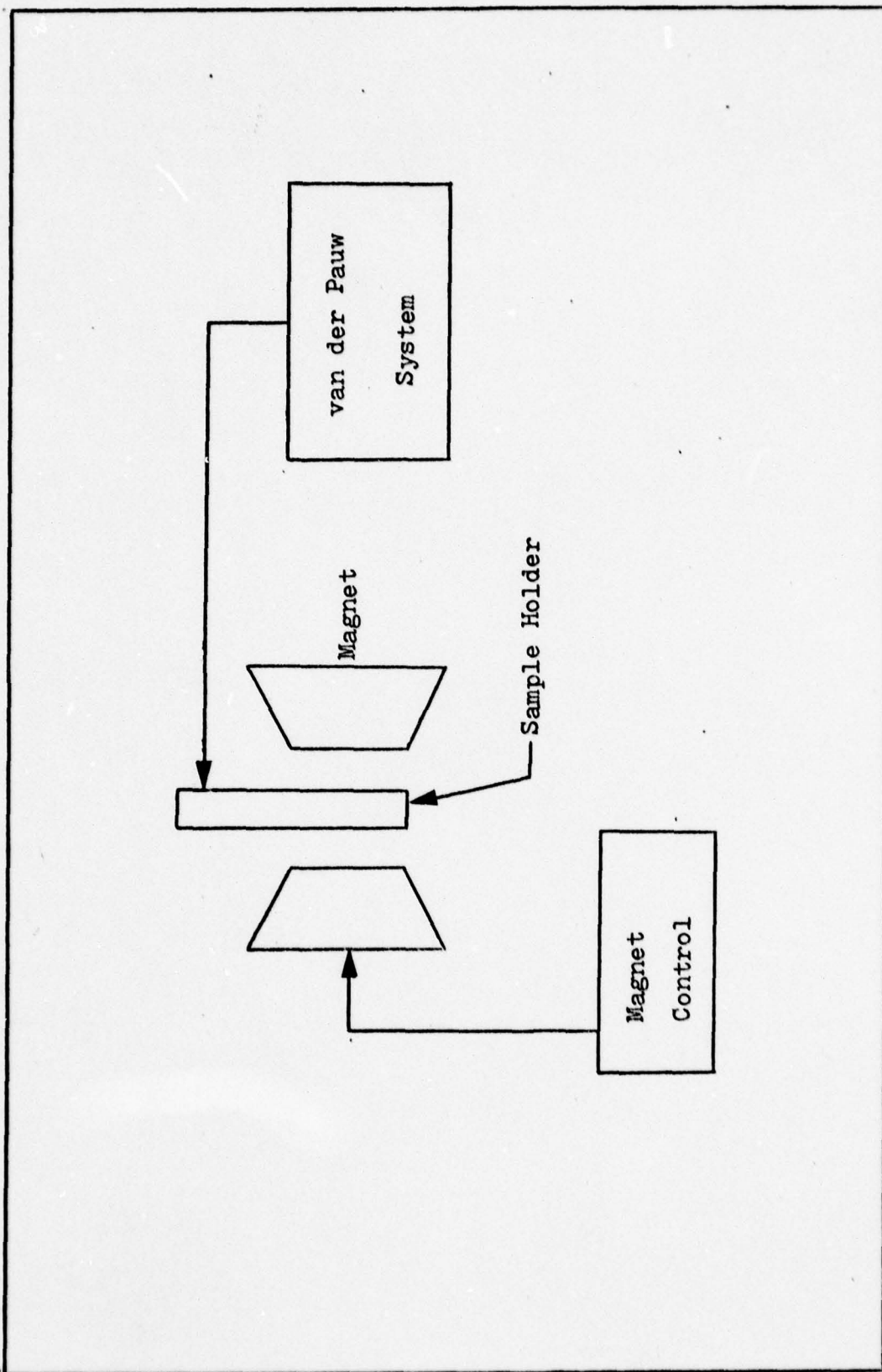


Fig. 7. Hall Measurement System

The stirred solution was required to prevent air bubbles from forming on the surface of the sample and causing an uneven etch. It was discovered later that the etching rate varied with the implant dose. A higher dose resulted in a higher rate of etch. Each sample was measured on a Sloan Dektak after the final etch to determine the total amount that had been removed from that sample. This was used to determine the etch rate for that individual chip. The slower stir rate was used to decrease the etch step for the higher implant doses. The rate of etch as a function of dose is depicted in Figure 8.

As previously mentioned, the samples were etched in a stirred solution. The samples were left on the sample holder during the etches. The krylon lacquer or black wax on the contacts protected them from the effects of the etching solution. The samples were etched and measured until they became too resistive to get accurate measurements or until the etched depth was much past the LSS theoretical limit of the implant. At this point the chip was removed from the sample holder and measured on the Dektak. The total amount that had been removed by the etching was determined by measuring the step between the protected contact areas and the etched area of the sample. The next sample was then mounted and measured as before.

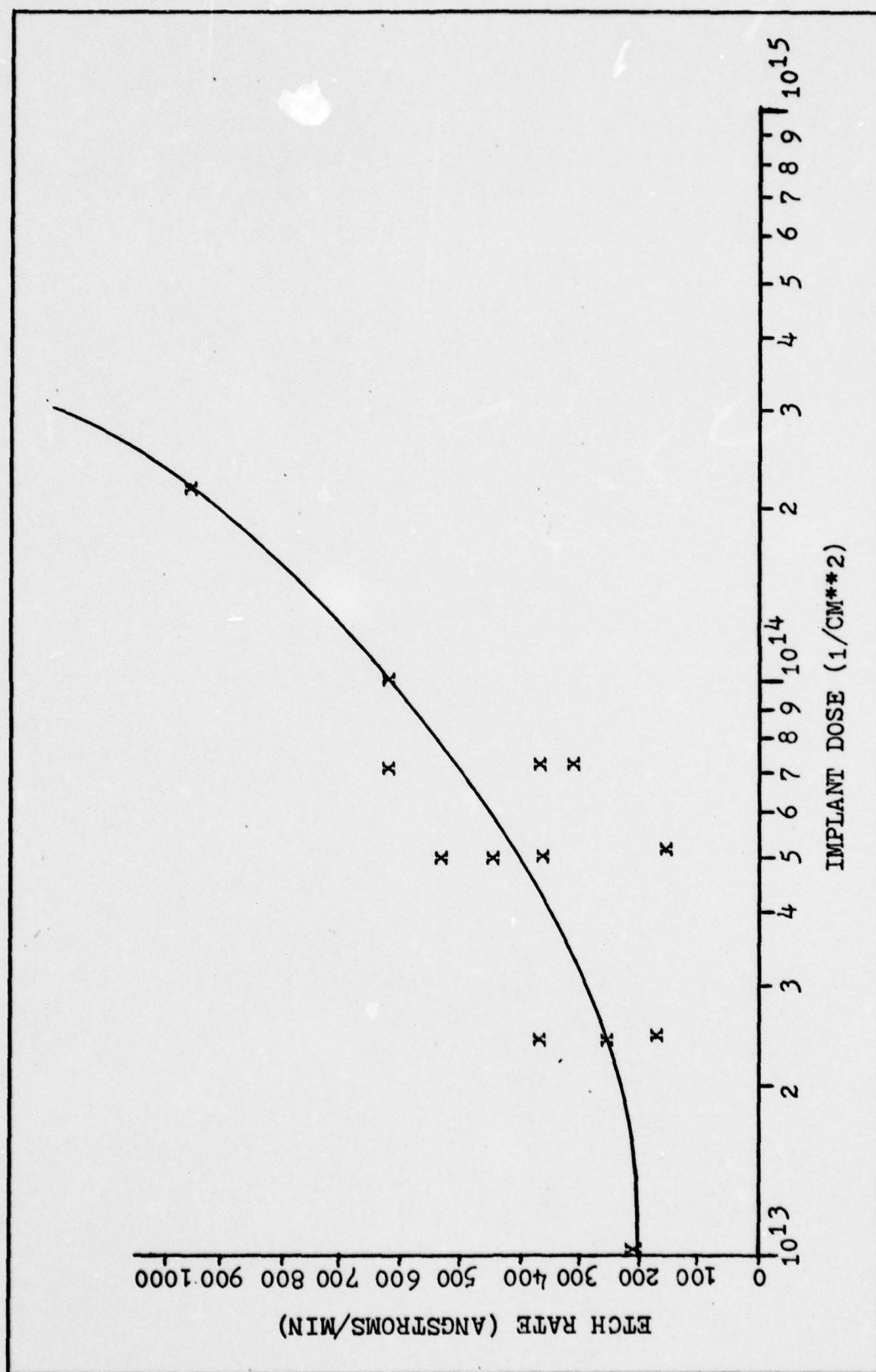


Fig. 8. Etch Rate vs Implant Dose

III. Experimental Results

This investigation generated a large amount of results. Some were as expected based on previous work and theory. A large percentage of the results, however, were contradictory to what had been expected. This section presents the results obtained in graphical and tabular form.

Several of the profile plots have only a few points on them and thus a true profile may not be presented. This was due to the unexpected high etch rate experienced with some of the samples. In a few cases, new samples were implanted with the same dose and profiled to correct for this problem. In most cases, the data were consistent. The few inconsistent plots were probably due to experimental error. Since the trend on the large majority of the profiles was a decreasing concentration and the GDOS plots are also decreasing, these plots would appear to be valid.

With the exception of sample S-1, all the profile plots have the same horizontal scale. This was done so that a better comparison could be made between the different plots.

Other information contained in this chapter include mobility and resistivity plots, efficiency vs implant dose graphs, and temperature and cap dependence graphs and tables.

TABLE I

Summary of Chips Profiled

Sample Number	Cap Type	Implant Dose	Carrier Density	Percent Efficiency
S - 1	Si_3N_4	1.0×10^{13}	4.39×10^{12}	44
S - 2	Si_3N_4	2.5×10^{13}	6.14×10^{12}	25
S - 3	Si_3N_4	5.0×10^{13}	7.98×10^{12}	16
S - 4	Si_3N_4	7.5×10^{13}	5.56×10^{12}	7
S - 5	Si_3N_4	1.0×10^{14}	1.06×10^{13}	11
S - 6	Si_3N_4	2.5×10^{14}	1.22×10^{13}	5
E - 3	Si_3N_4	5.0×10^{13}	6.76×10^{12}	14
E - 4	Si_3N_4	7.5×10^{13}	9.50×10^{12}	13
N - 2	Si_3N_4	5.0×10^{13}	9.46×10^{12}	19
N - 3	Si_3N_4	7.5×10^{13}	1.35×10^{13}	18
N - 4	Si_3N_4	1.0×10^{14}	1.06×10^{13}	11
C - 1	Si_3N_4 SiO_2	5.0×10^{13}	8.71×10^{12}	17
C - 3	Al_2O_3	5.0×10^{13}	3.91×10^{12}	8

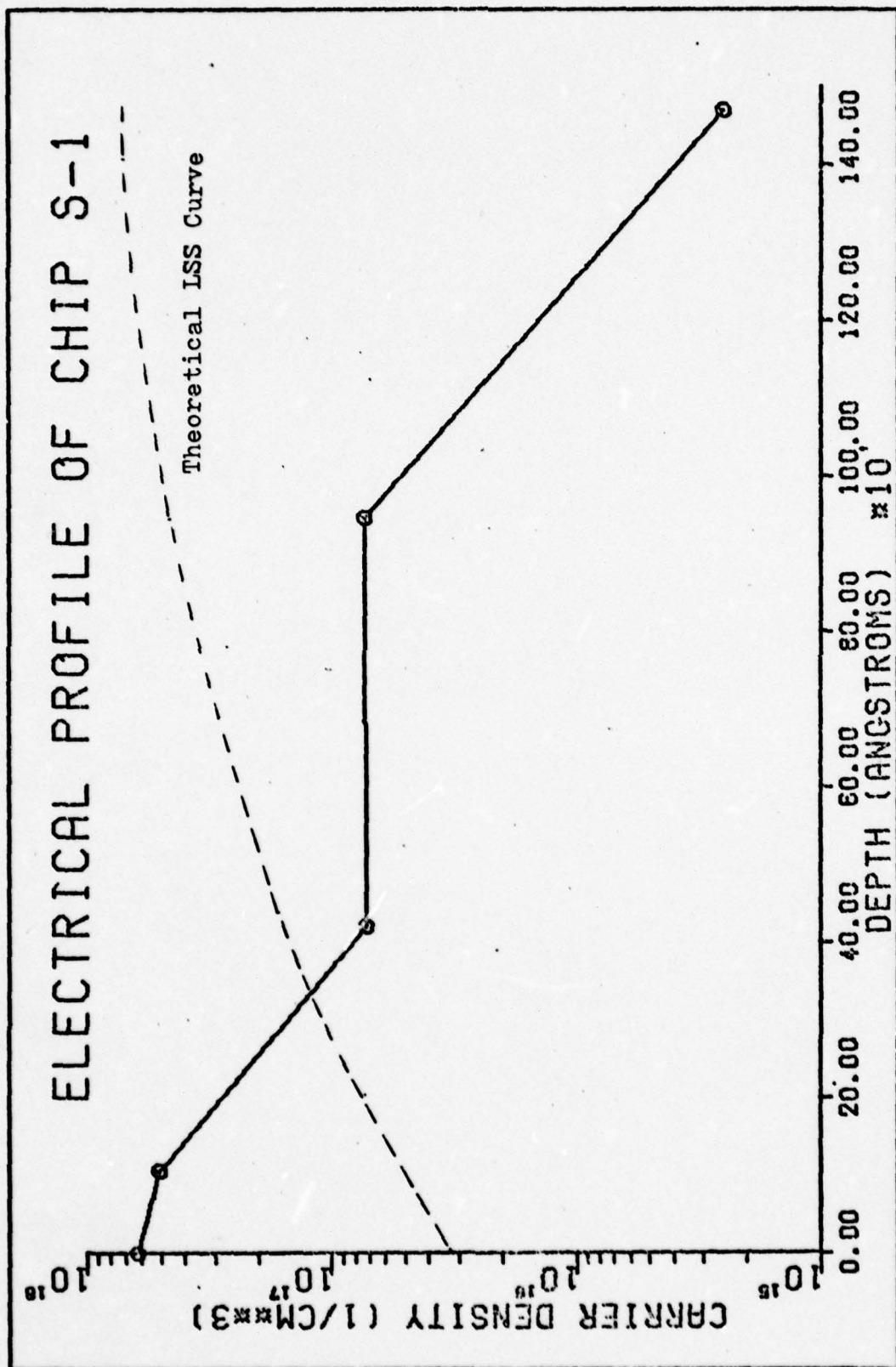


Fig. 9. Differential Hall Profile of Sample S-1

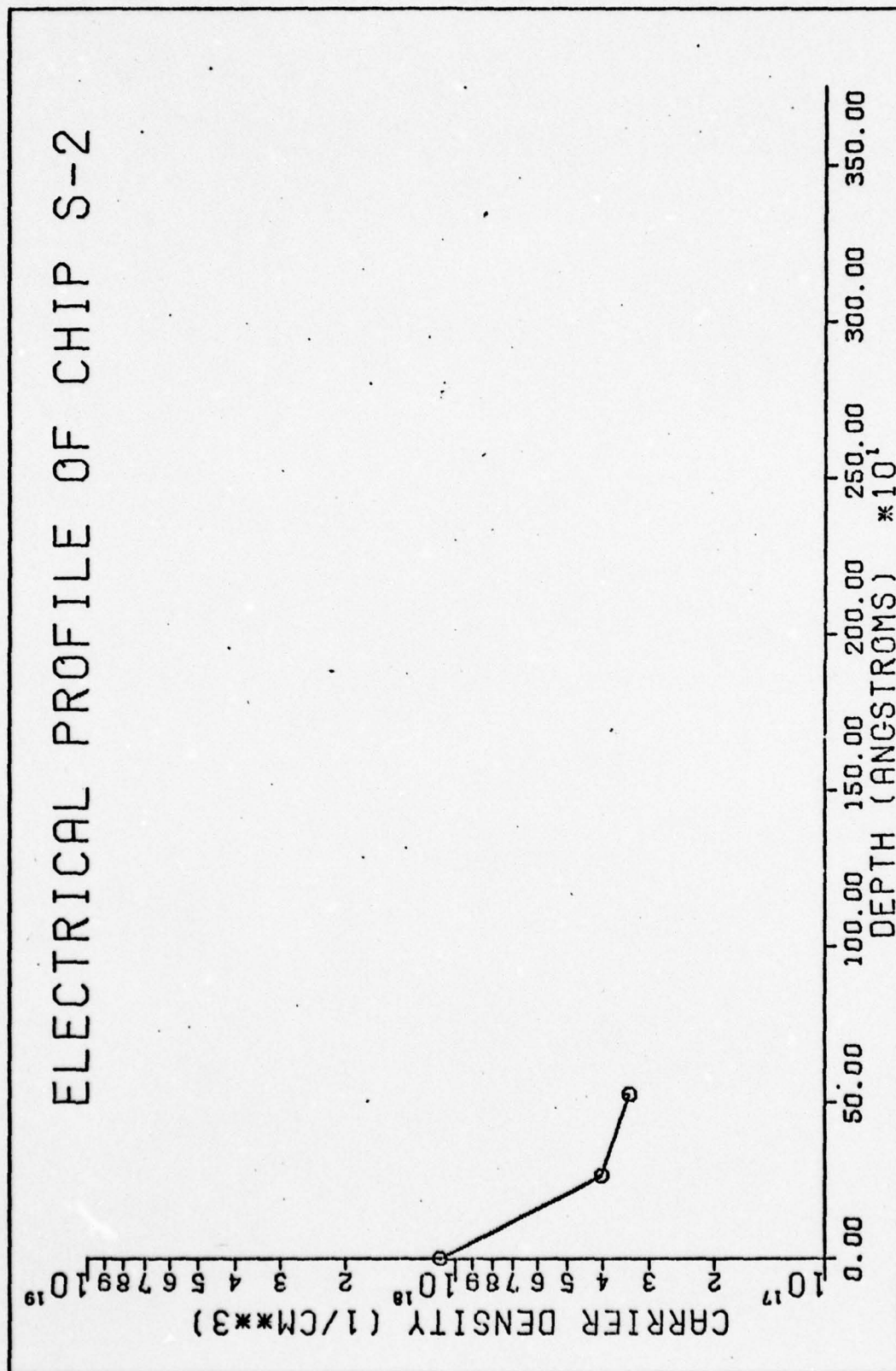


Fig. 10. Differential Hall Profile of Sample S-2

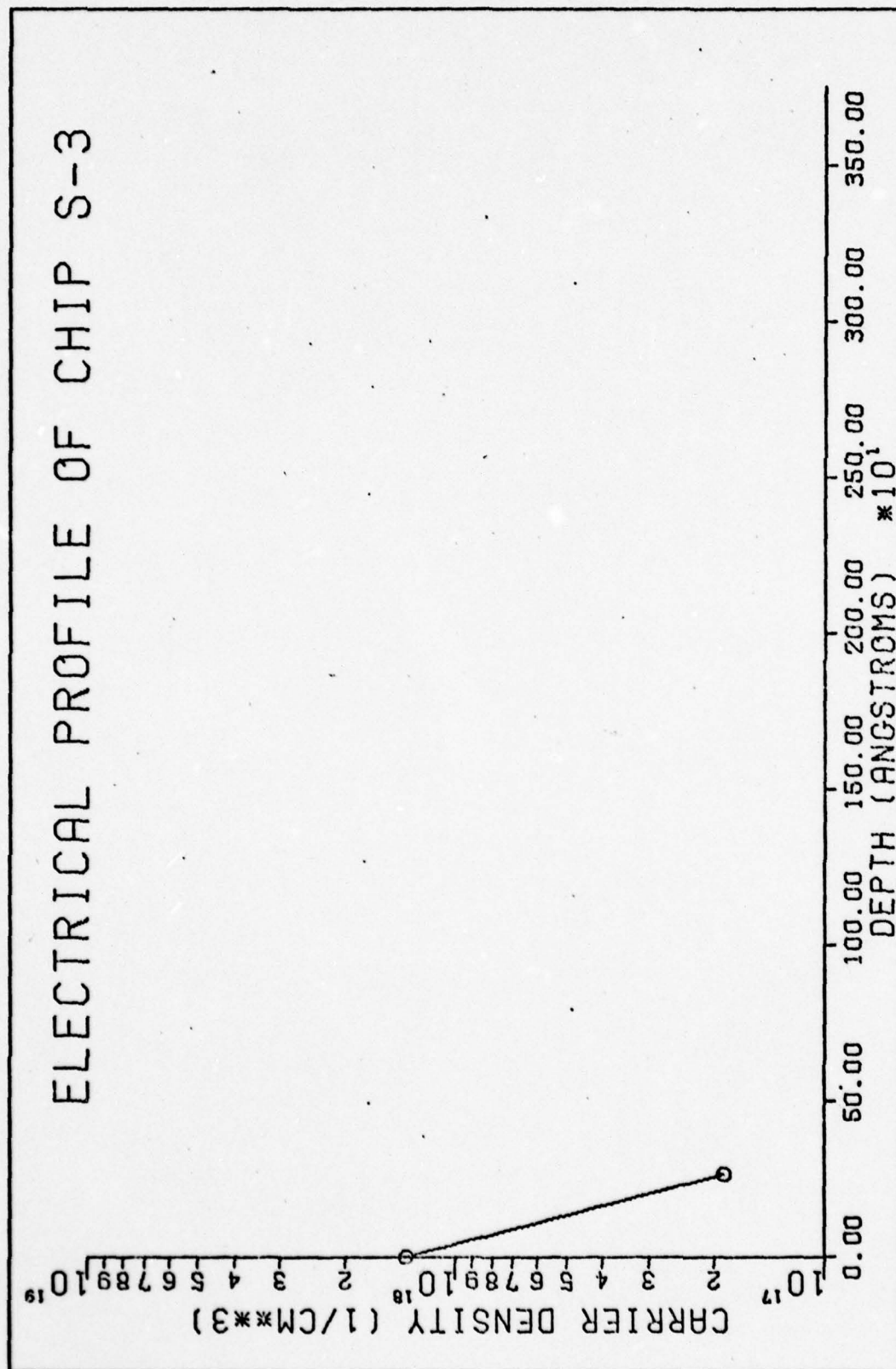


Fig. 11. Differential Hall Profile of Sample S-3

ELECTRICAL PROFILE OF CHIP S-4

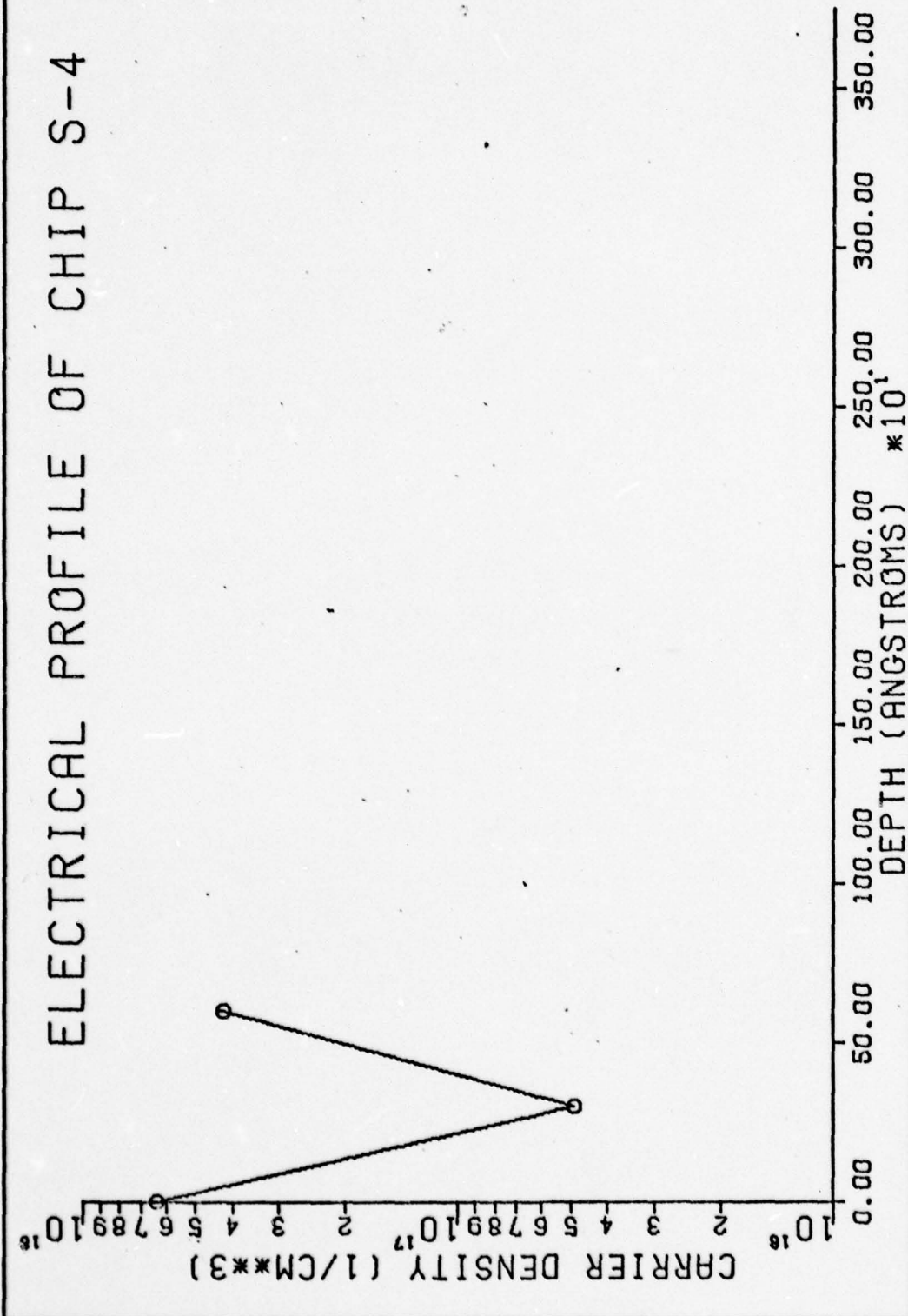


Fig. 12. Differential Hall Profile of Sample S-4

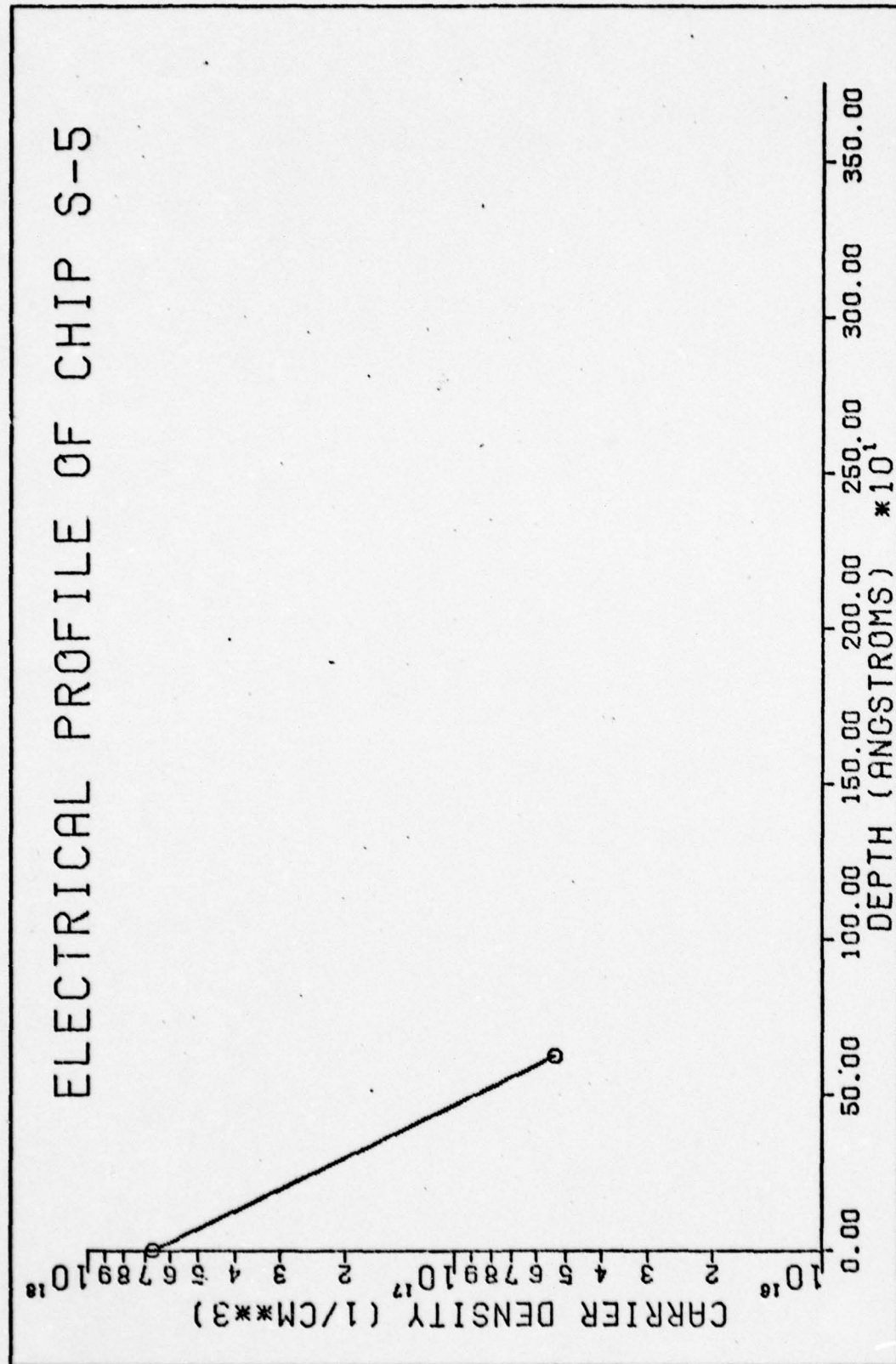


Fig. 13. Differential Hall Profile of Sample S-5

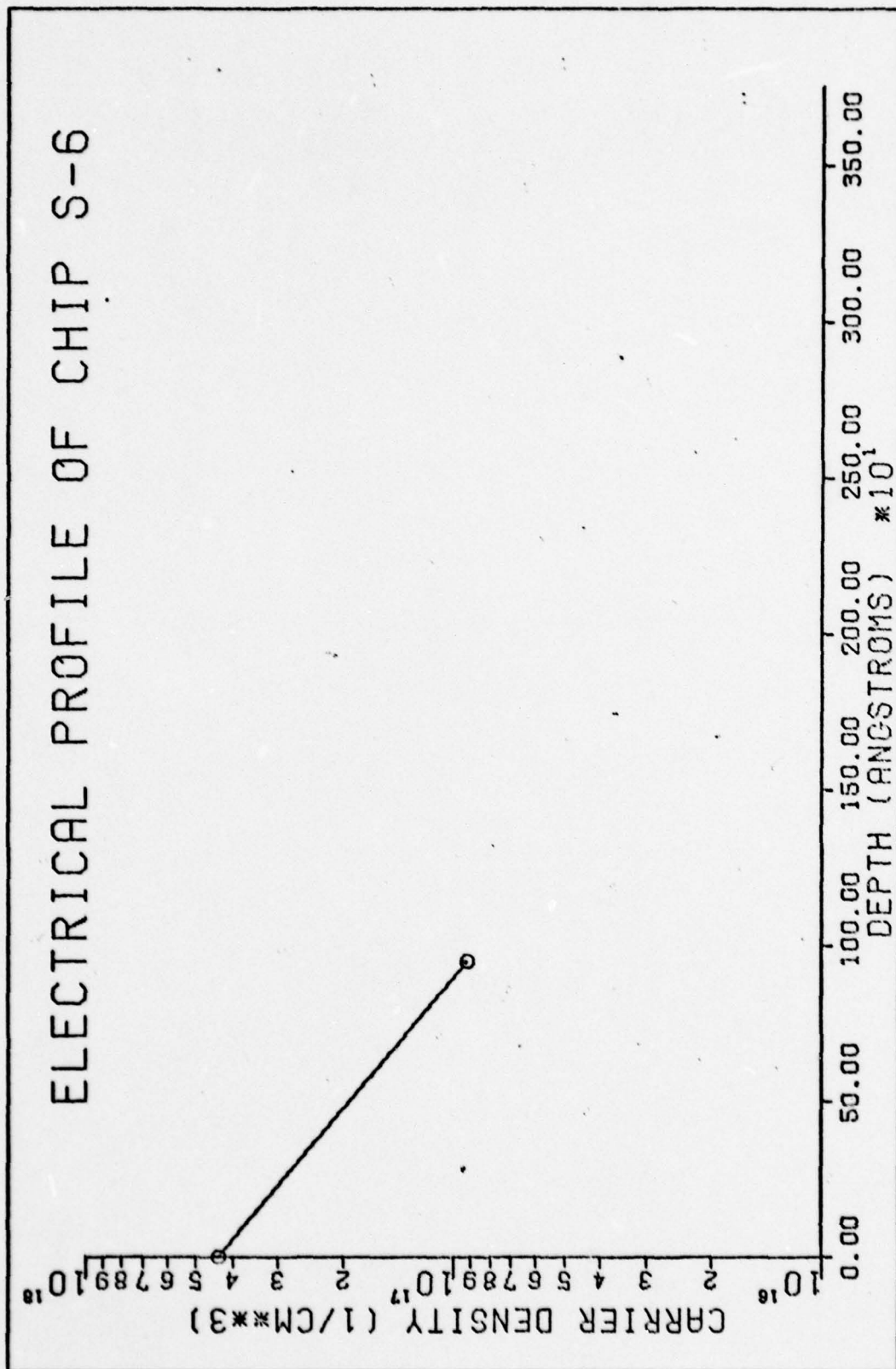


Fig. 14. Differential Hall Profile of Sample S-6

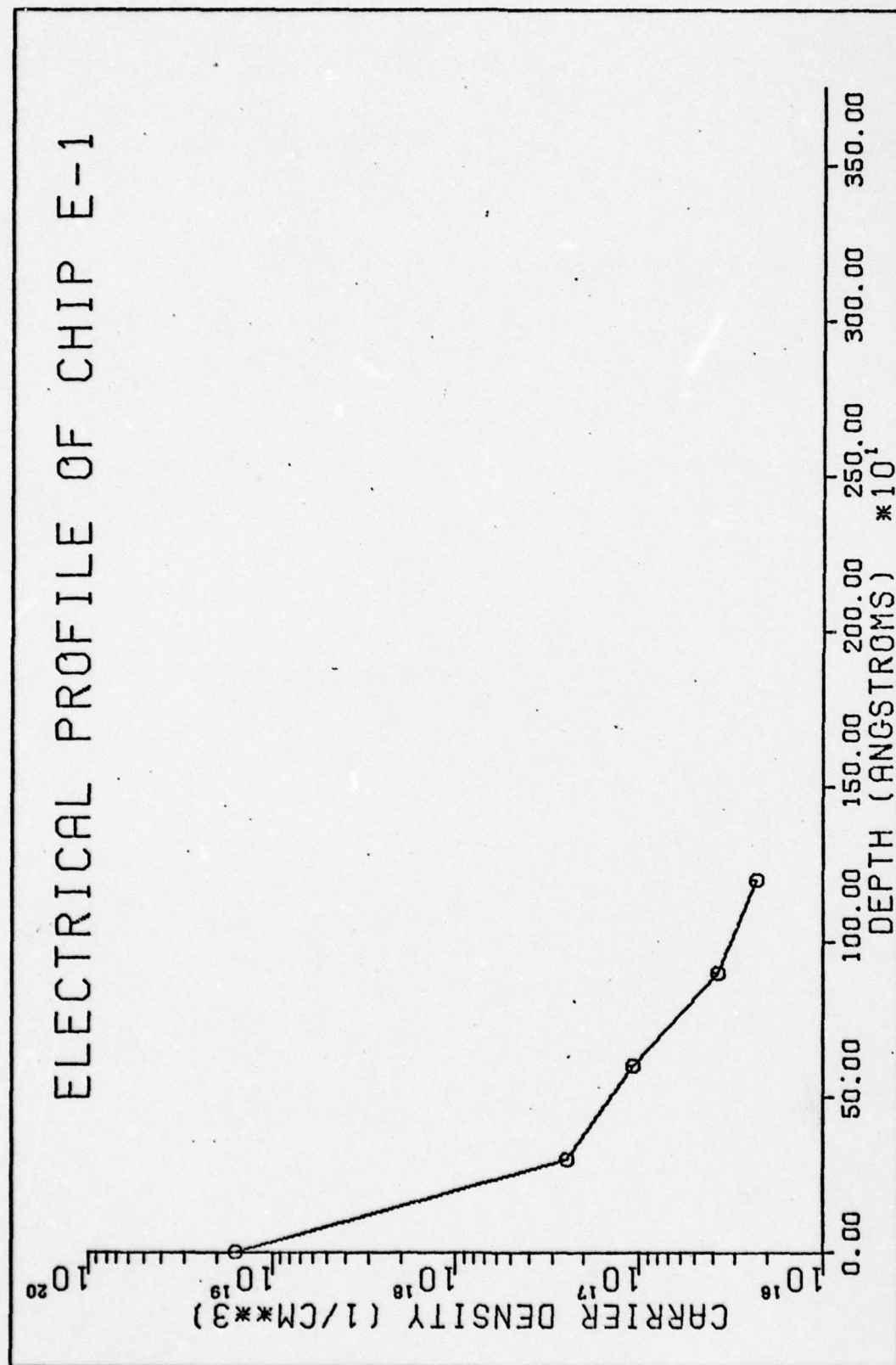


Fig. 15. Differential Hall Profile of Sample E-1

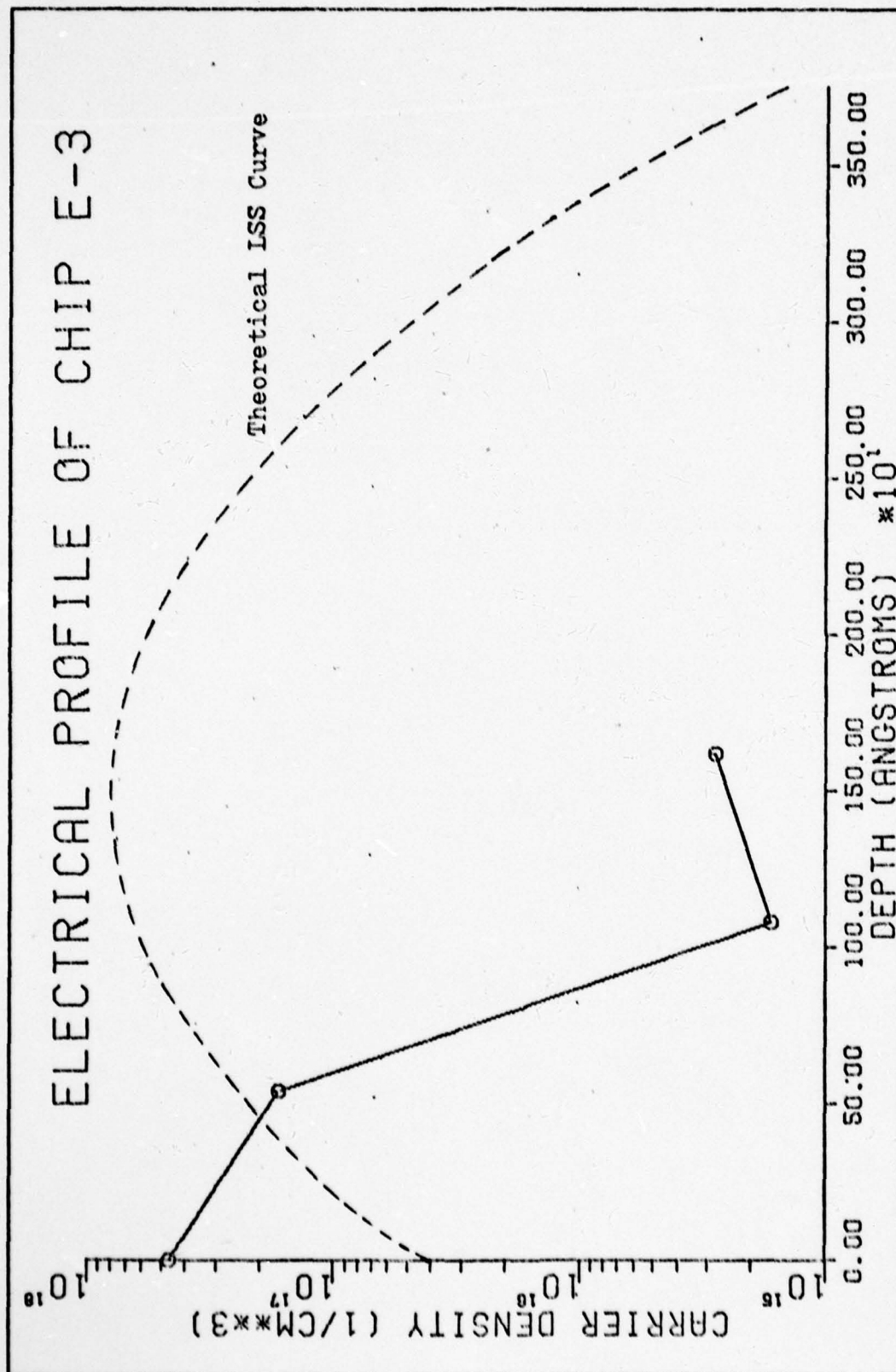


Fig. 16. Differential Hall Profile of Sample E-3

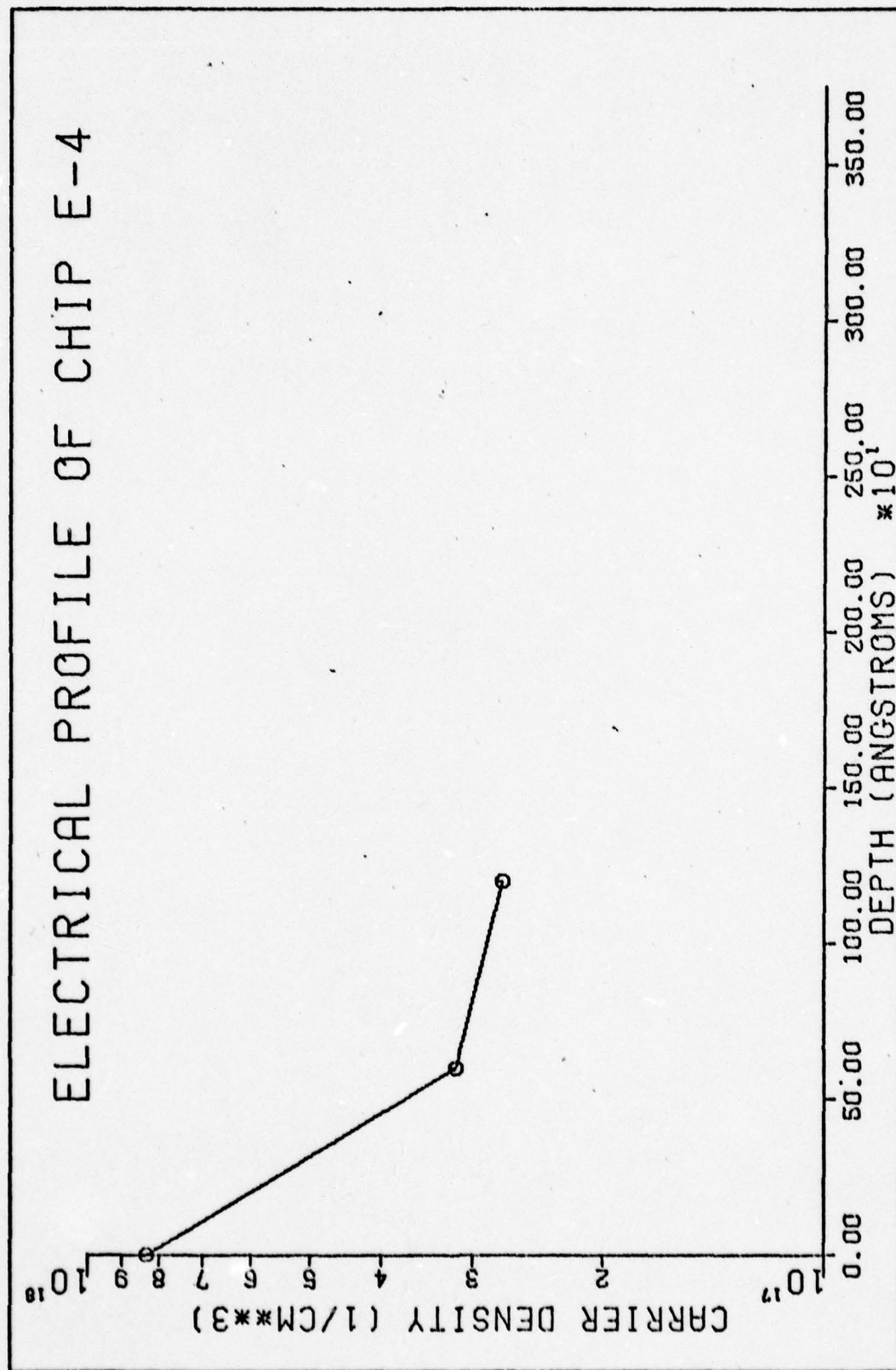


Fig. 17. Differential Hall Profile of Sample E-4

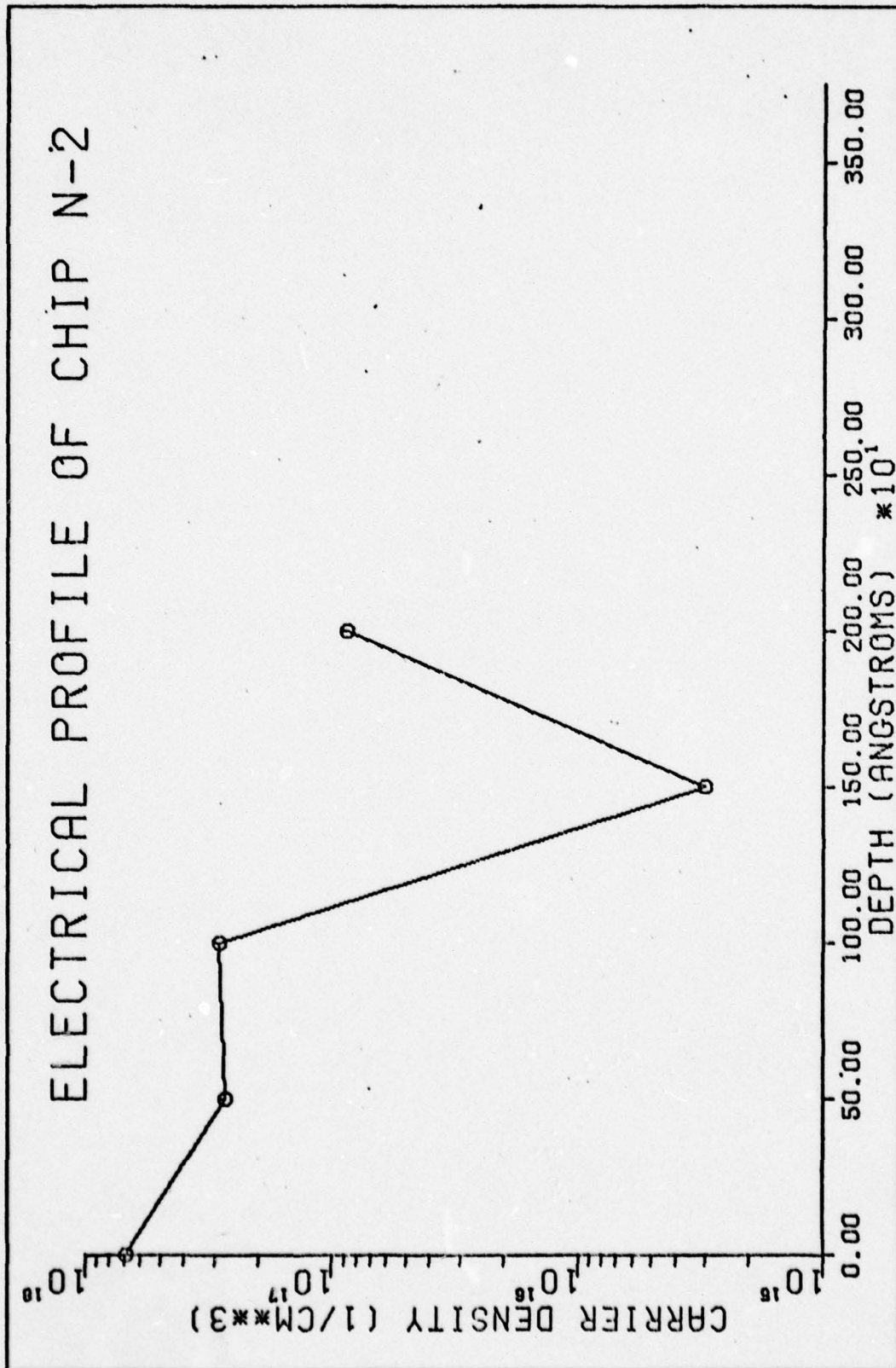


Fig. 18. Differential Hall Profile of Sample N-2

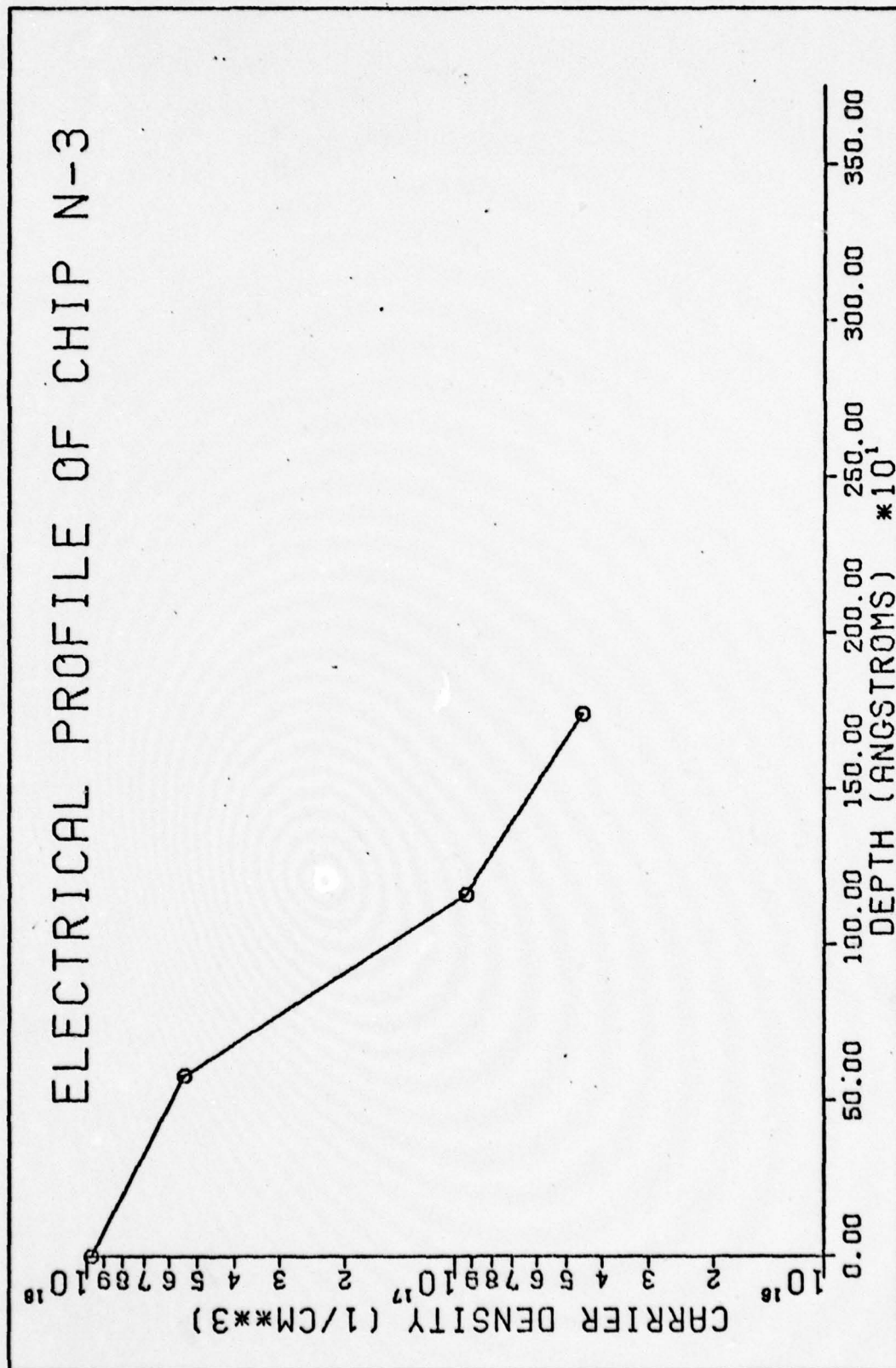


Fig. 19. Differential Hall Profile of Sample N-3

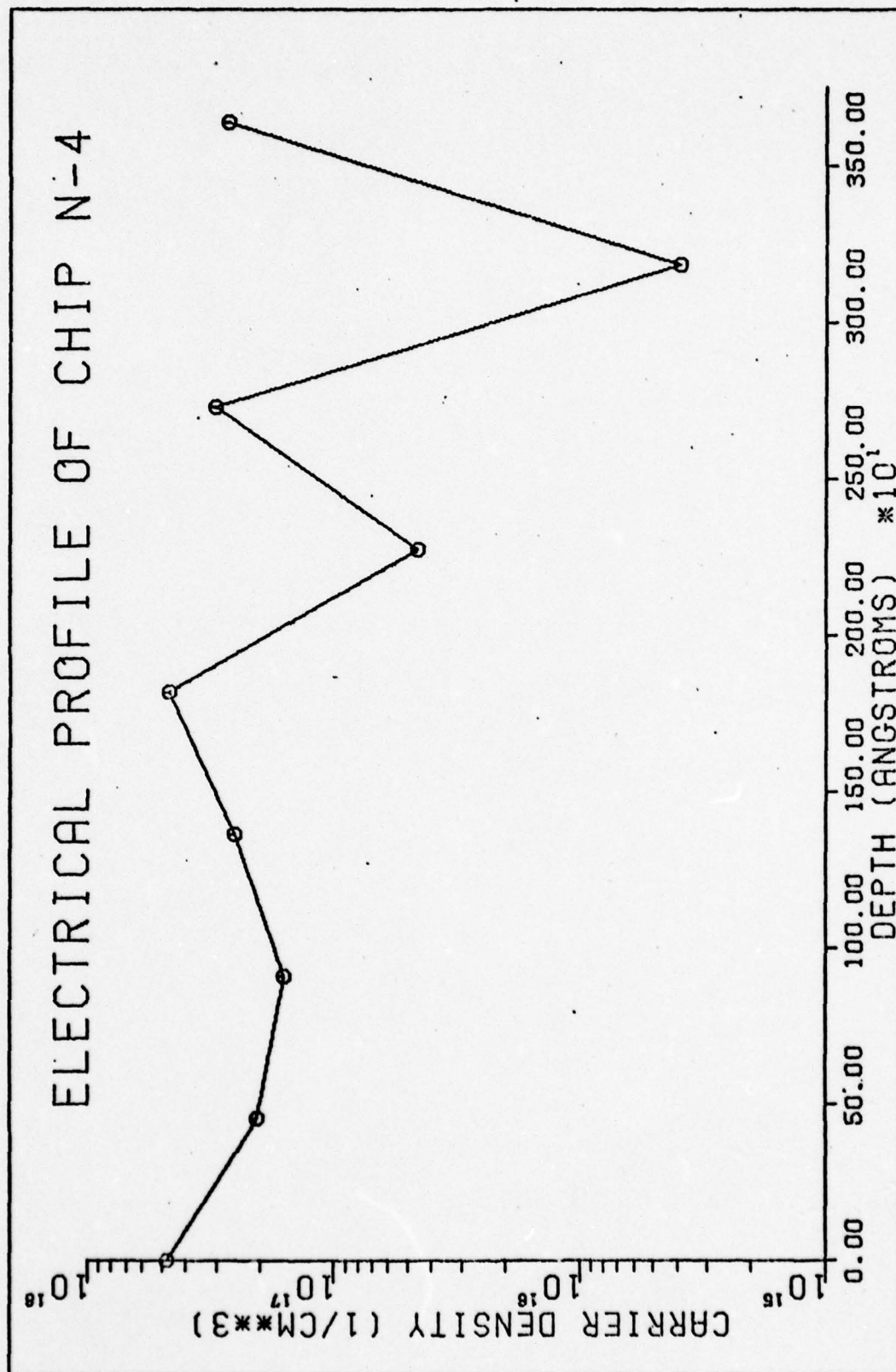


Fig. 20. Differential Hall Profile of Sample N-4

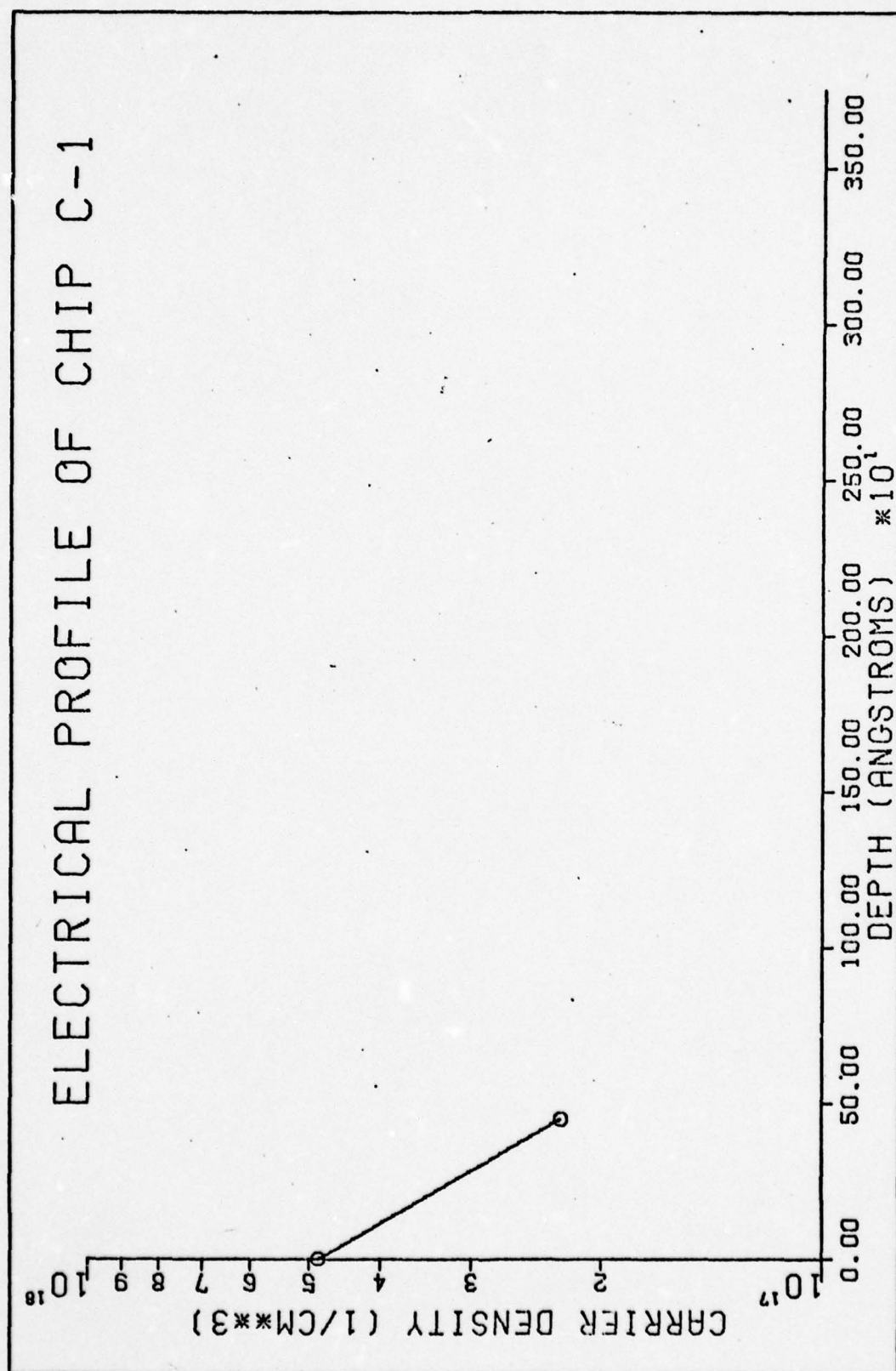


Fig. 21. Differential Hall Profile of Sample C-1

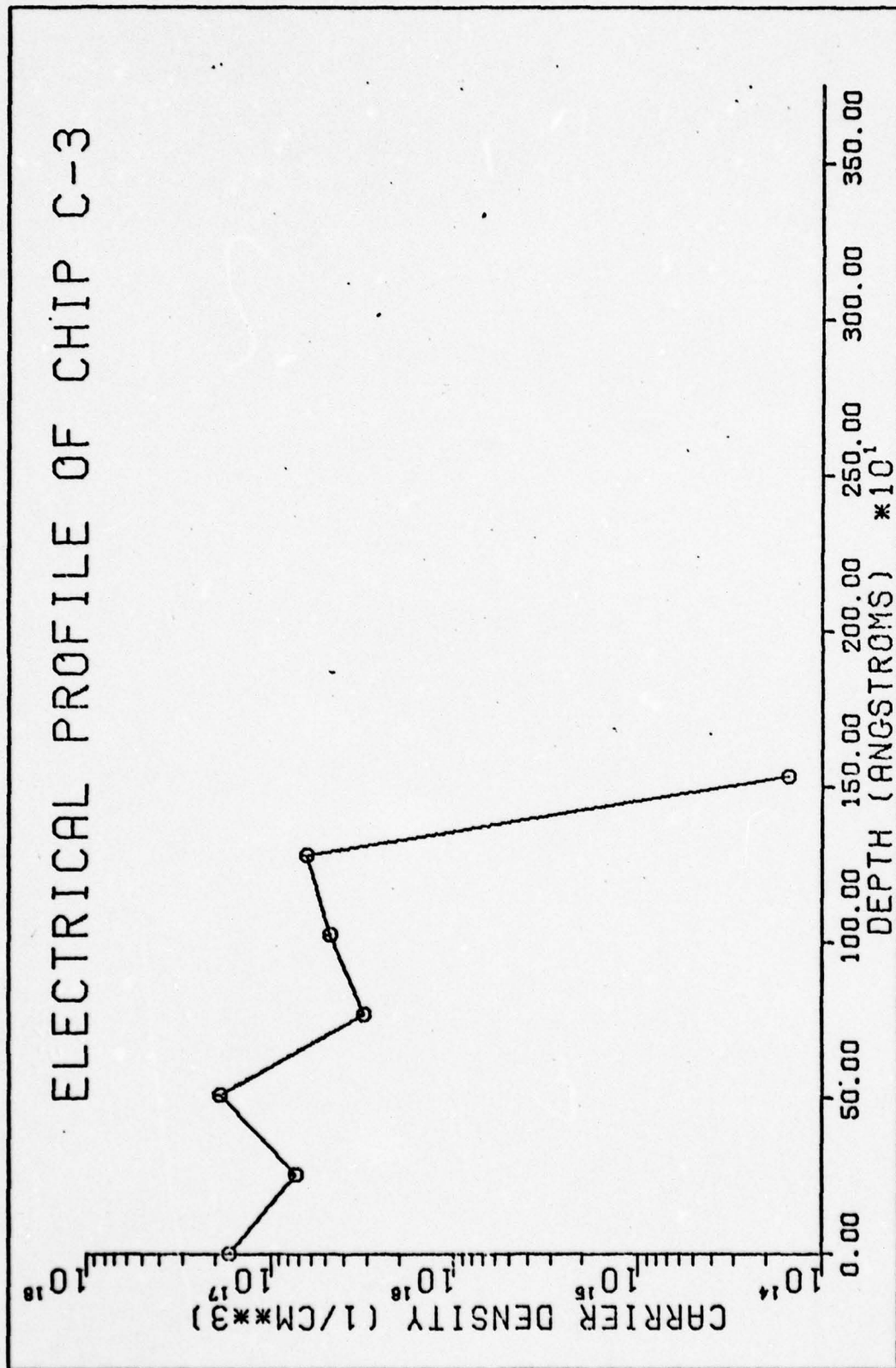


Fig. 22. Differential Hall Profile of Sample C-3

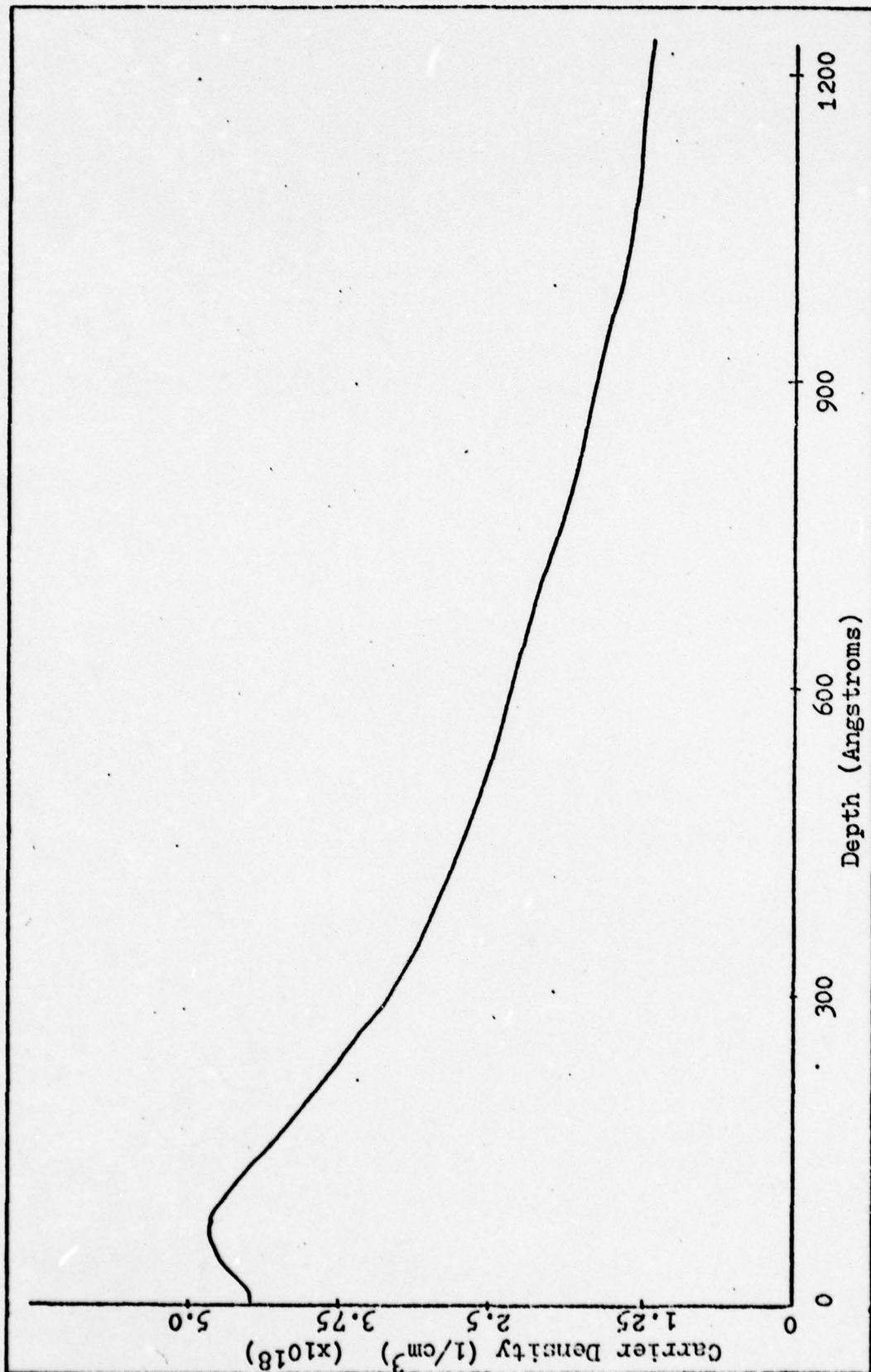


Fig. 23. Glow Discharge Optical Spectrography Profile of Mg Implanted ($10^{15}/\text{cm}^2$) GaP

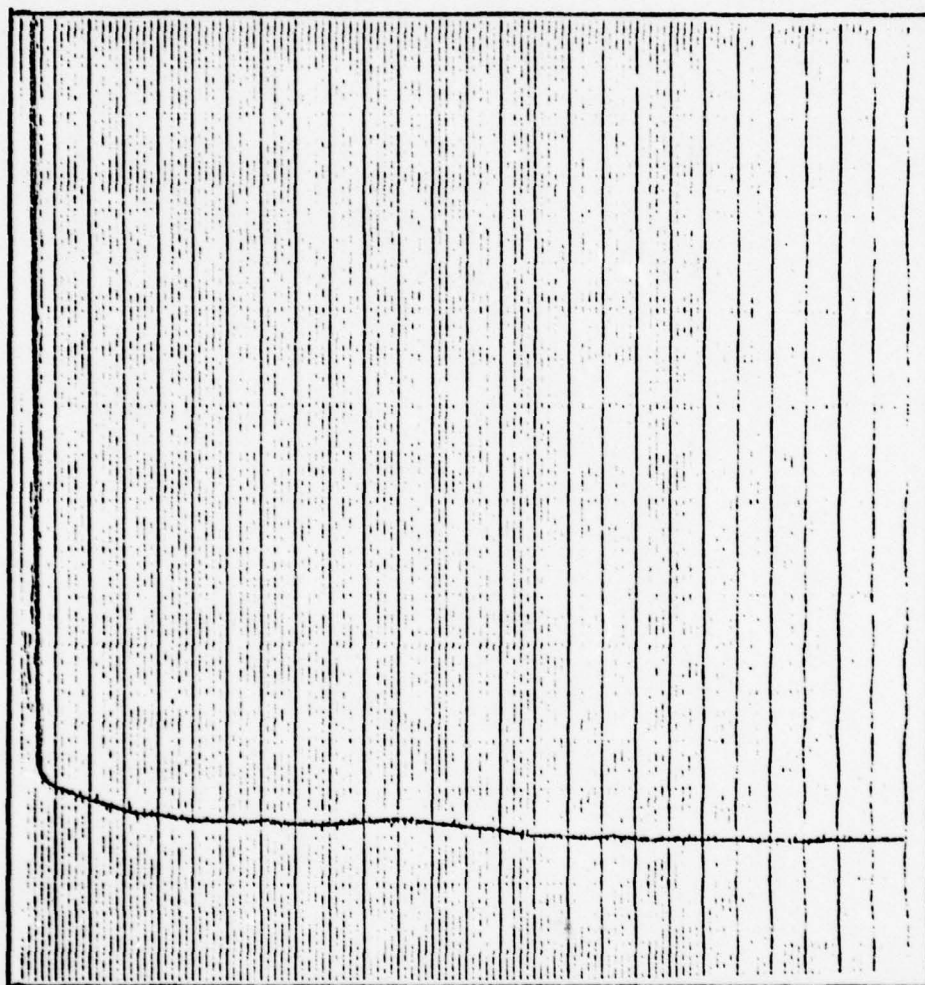


Fig. 24. GDOS Profile of Mg Implanted GaP (1×10^{15})

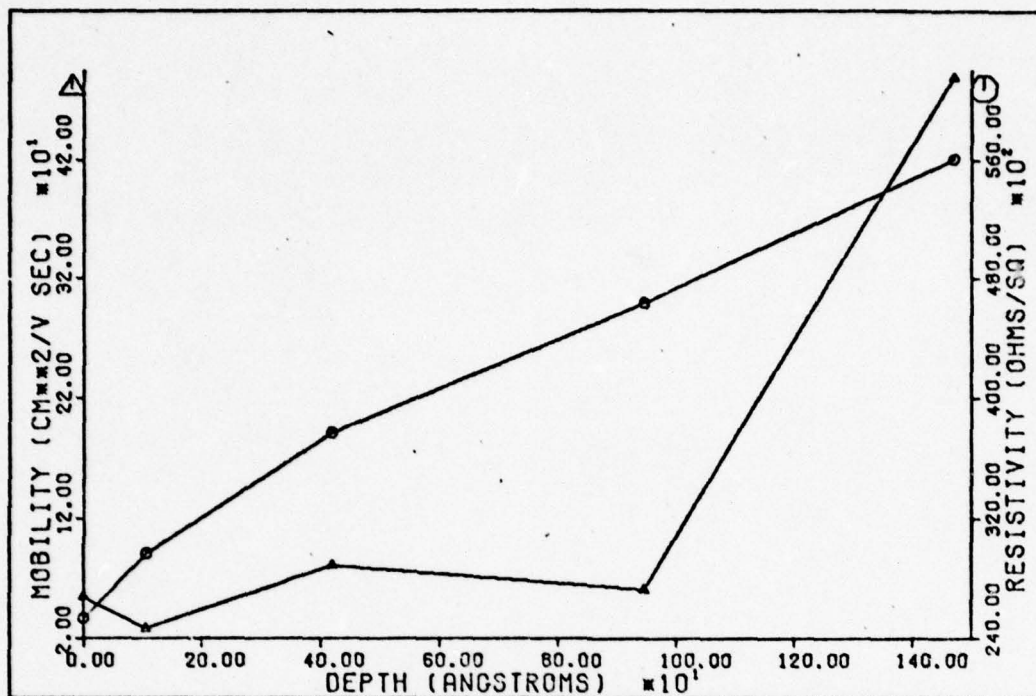


Fig. 25. Mobility and Resistivity Plots for Sample S-1

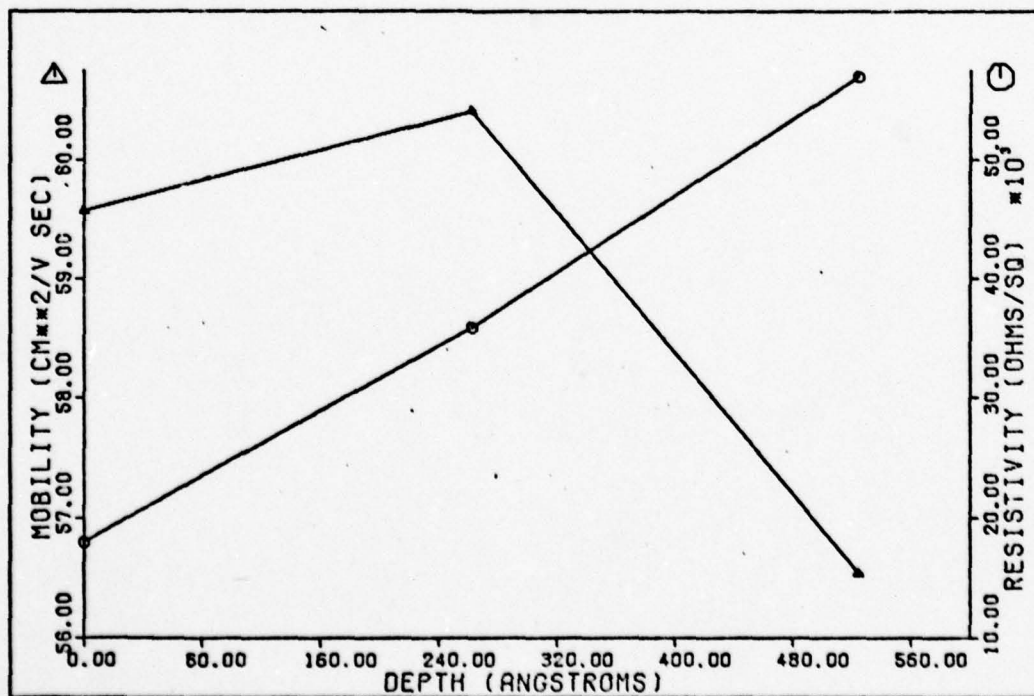


Fig. 26. Mobility and Resistivity Plots for Sample S-2

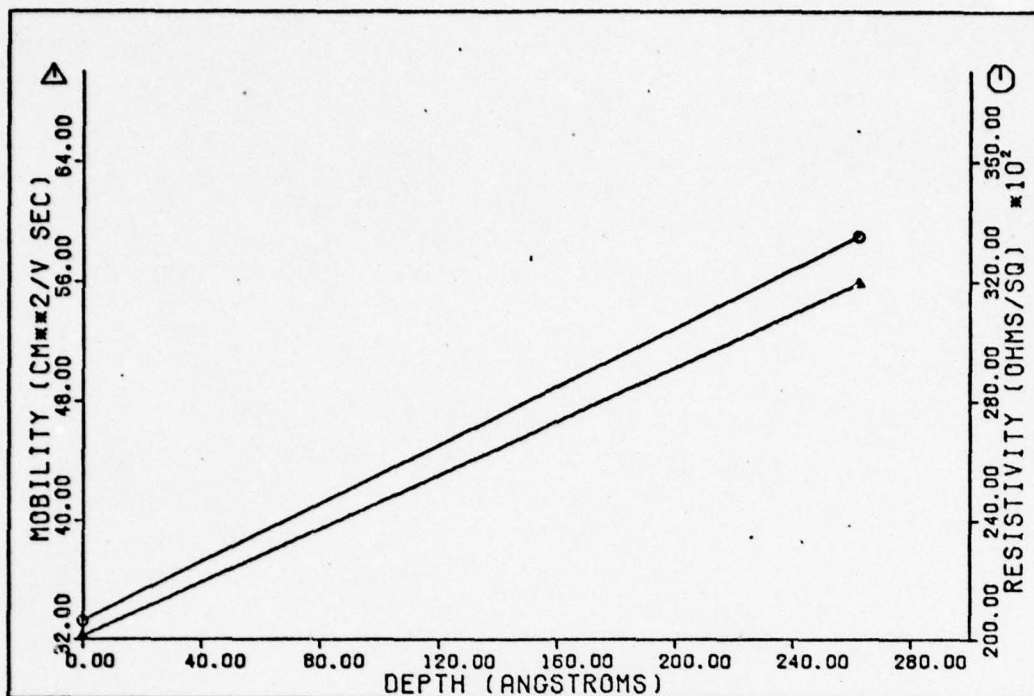


Fig. 27. Mobility and Resistivity Plots for Sample S-3

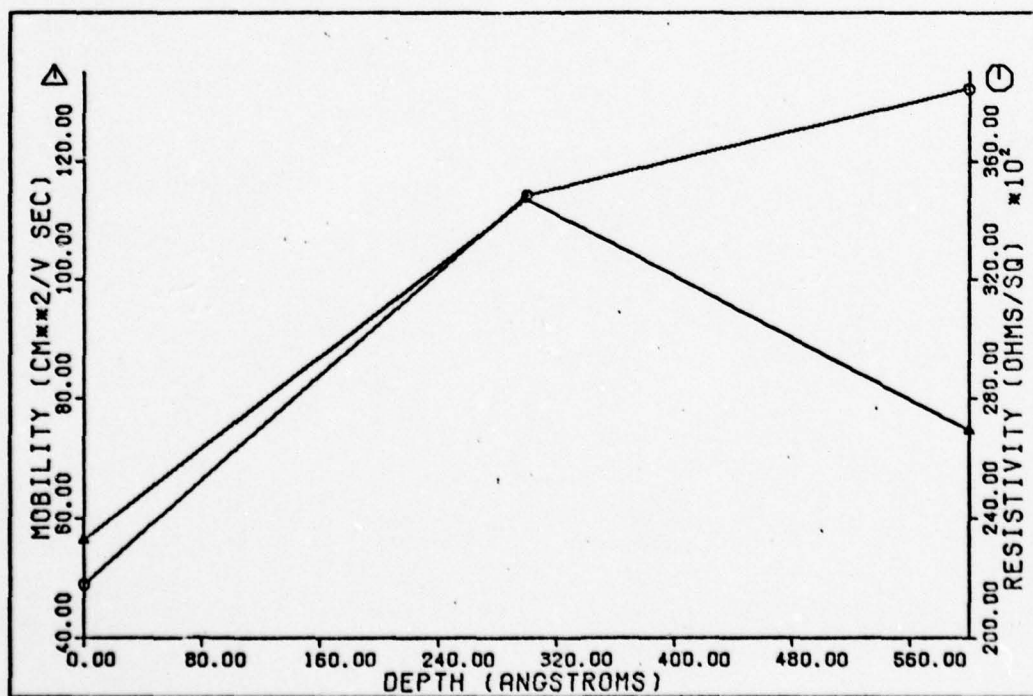


Fig. 28. Mobility and Resistivity Plots for Sample S-4

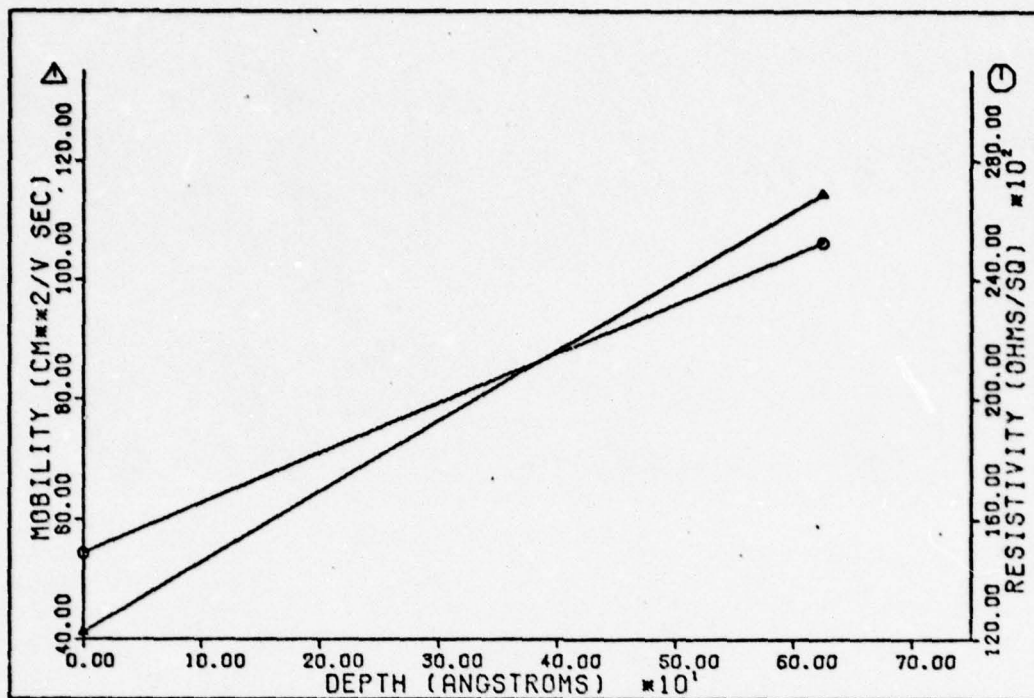


Fig. 29. Mobility and Resistivity Plots for Sample S-5

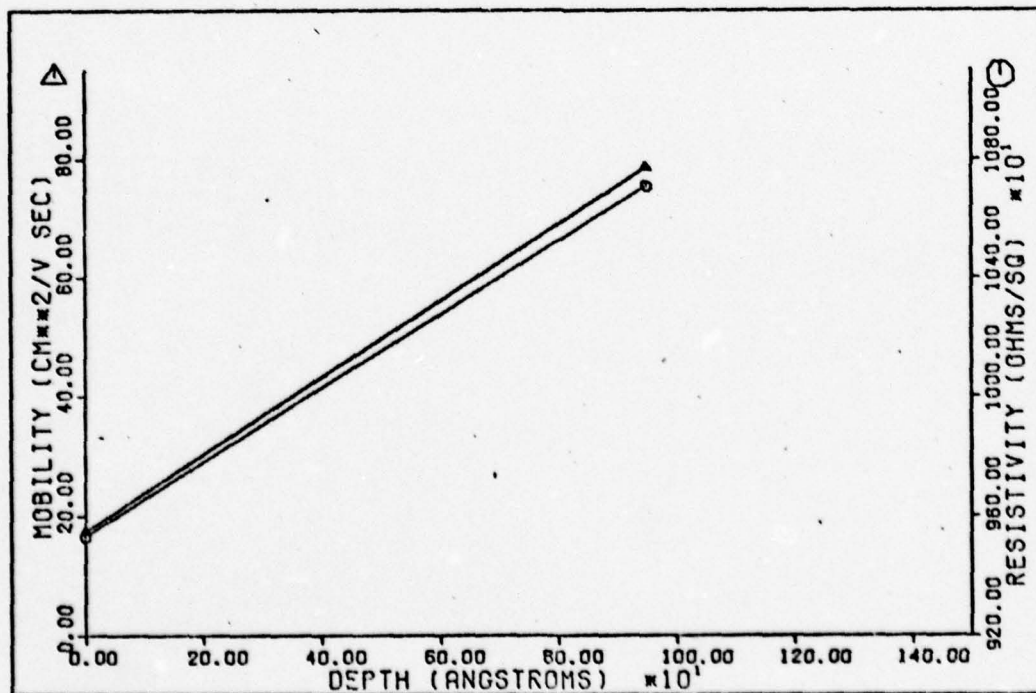


Fig. 30. Mobility and Resistivity Plots for Sample S-6

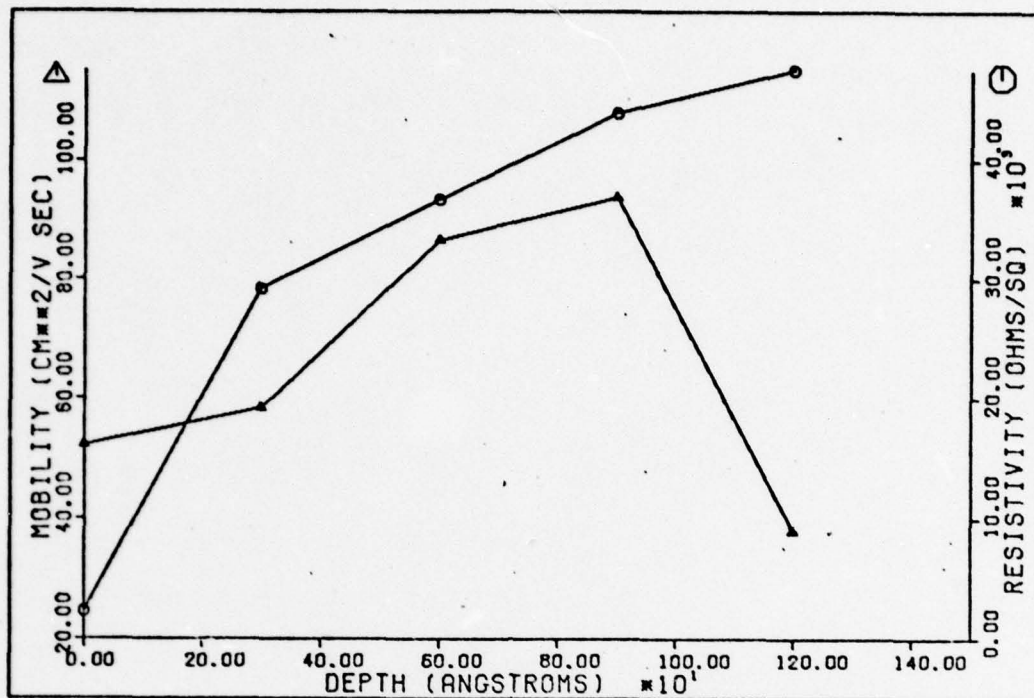


Fig. 31. Mobility and Resistivity Plots for Sample E-1

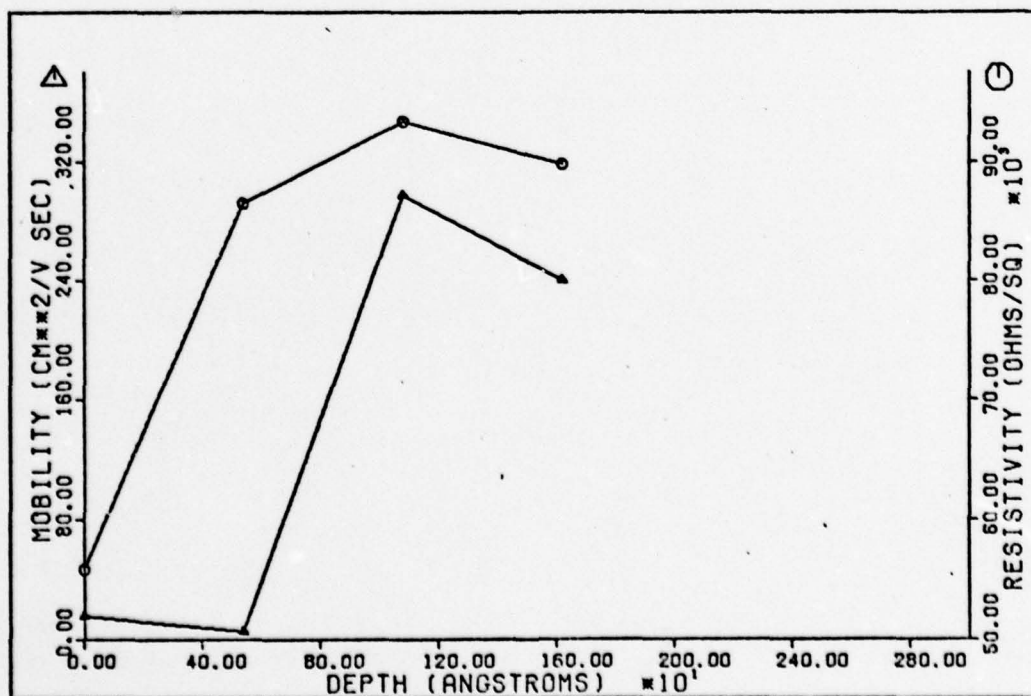


Fig. 32. Mobility and Resistivity Plots for Sample E-3

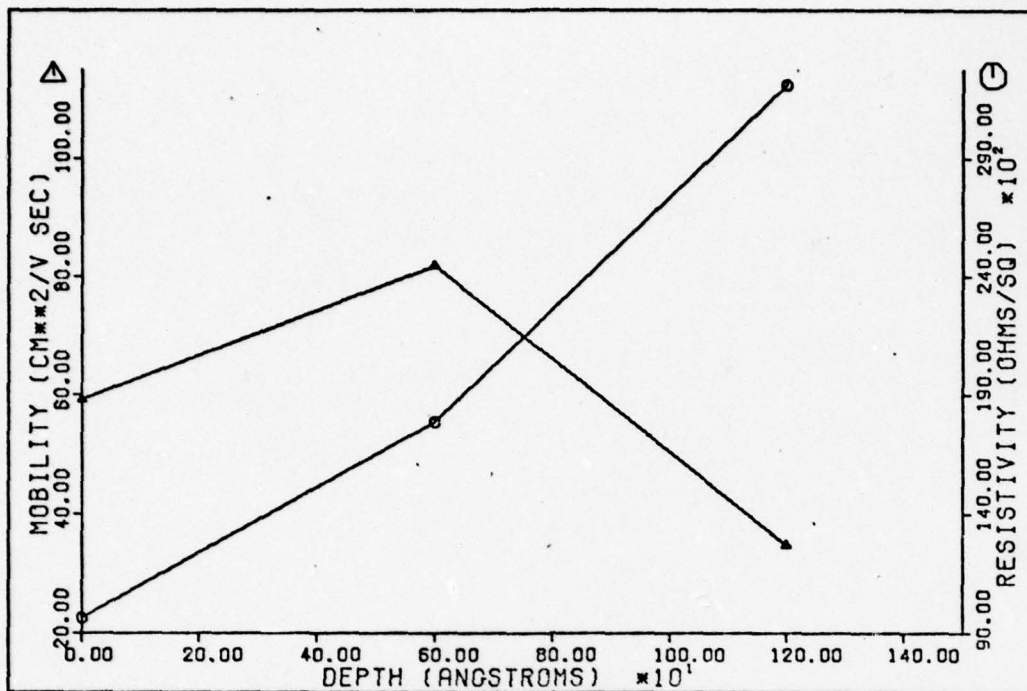


Fig. 33. Mobility and Resistivity Plots for Sample E-4

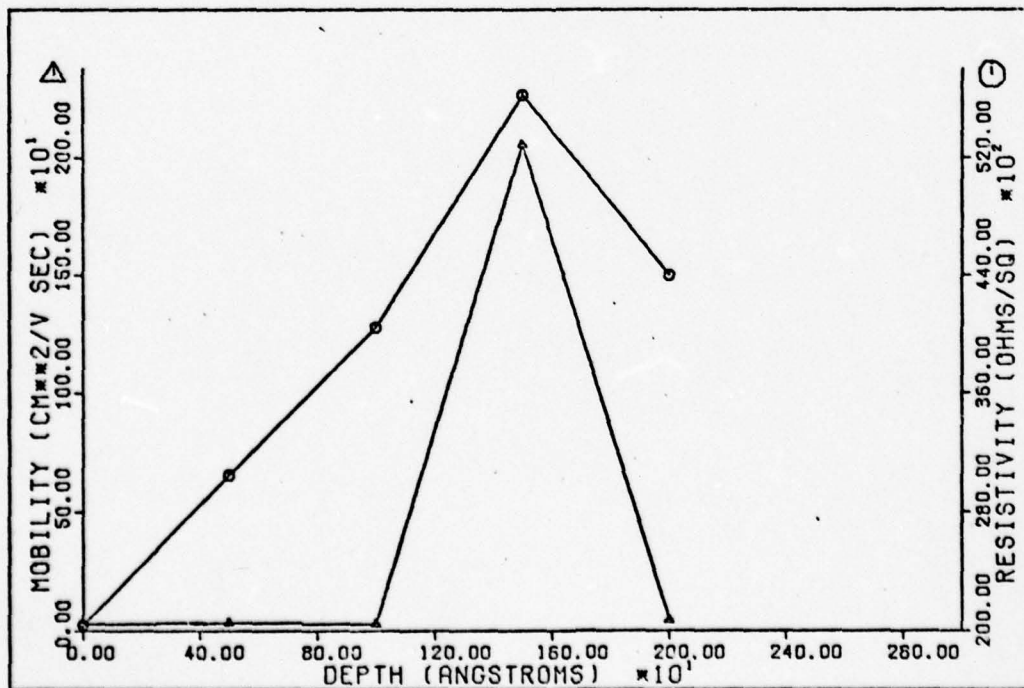


Fig. 34. Mobility and Resistivity Plots for Sample N-2

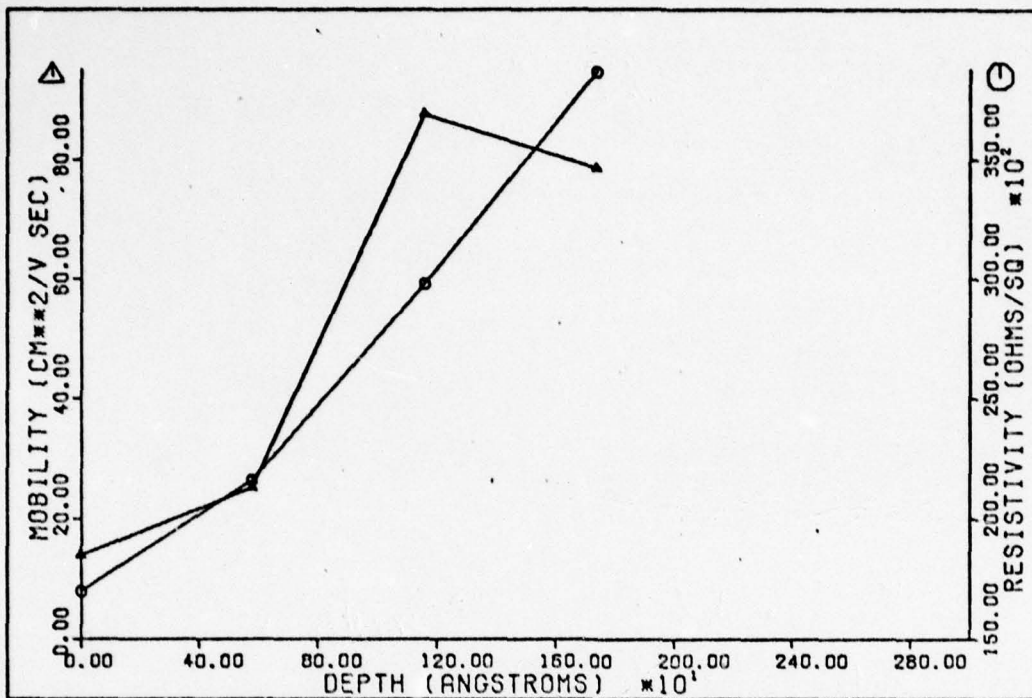


Fig. 35. Mobility and Resistivity Plots for Sample N-3

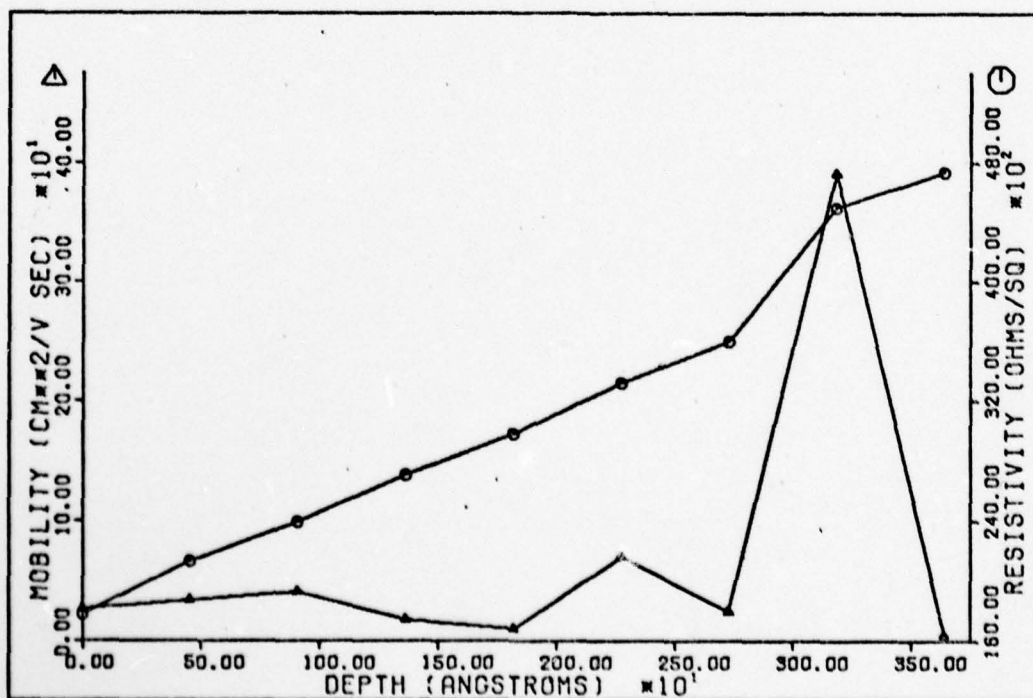


Fig. 36. Mobility and Resistivity Plots for Sample N-4

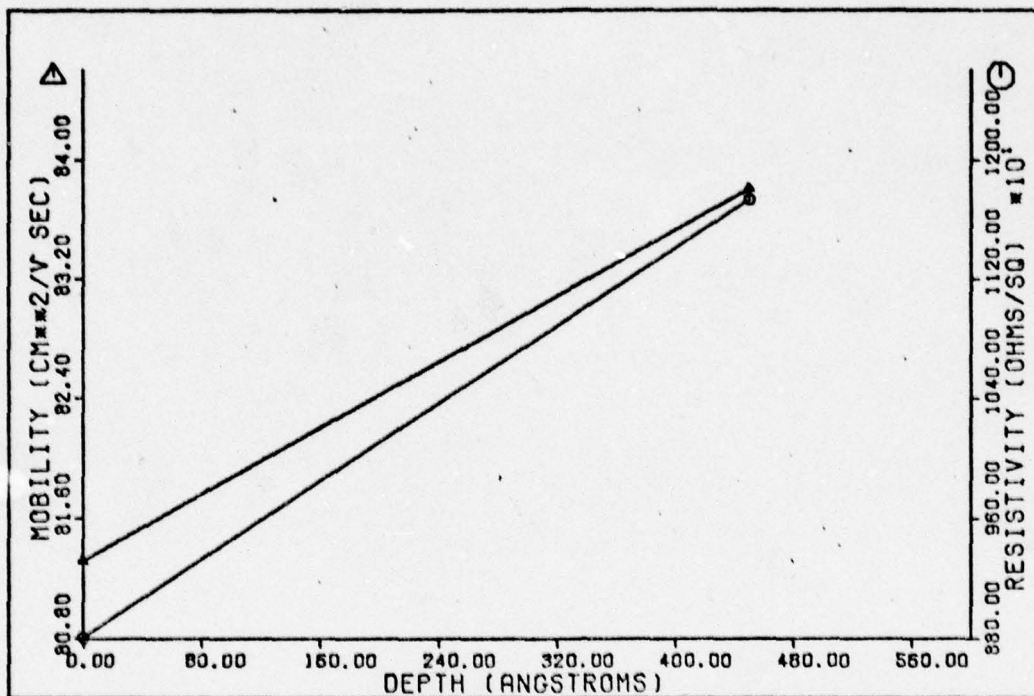


Fig. 37. Mobility and Resistivity Plots for Sample C-1

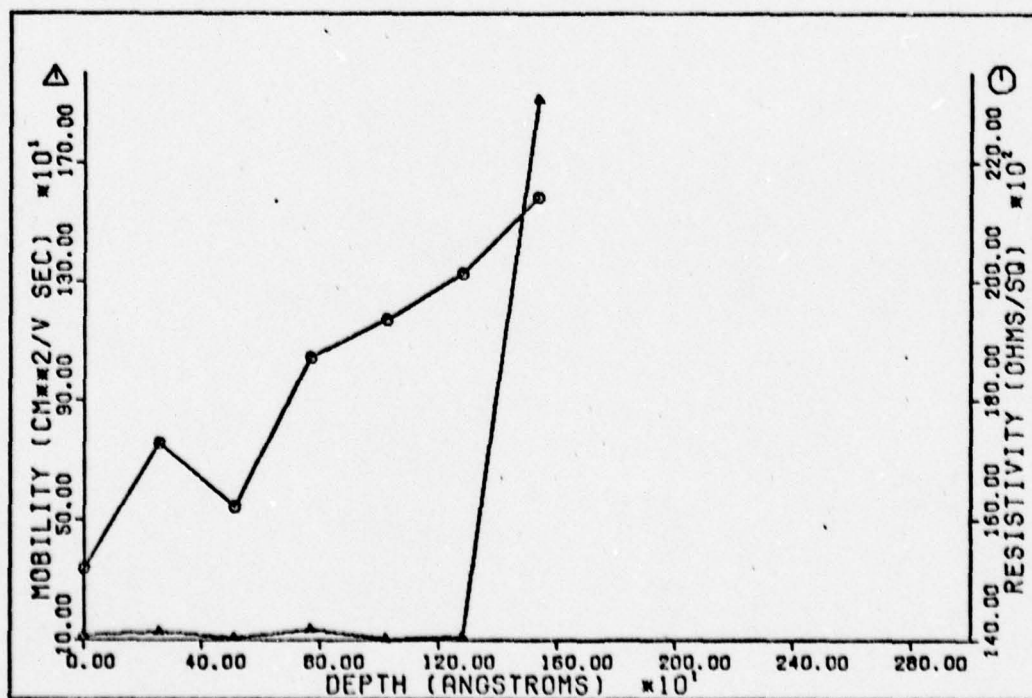


Fig. 38. Mobility and Resistivity Plots for Sample C-3

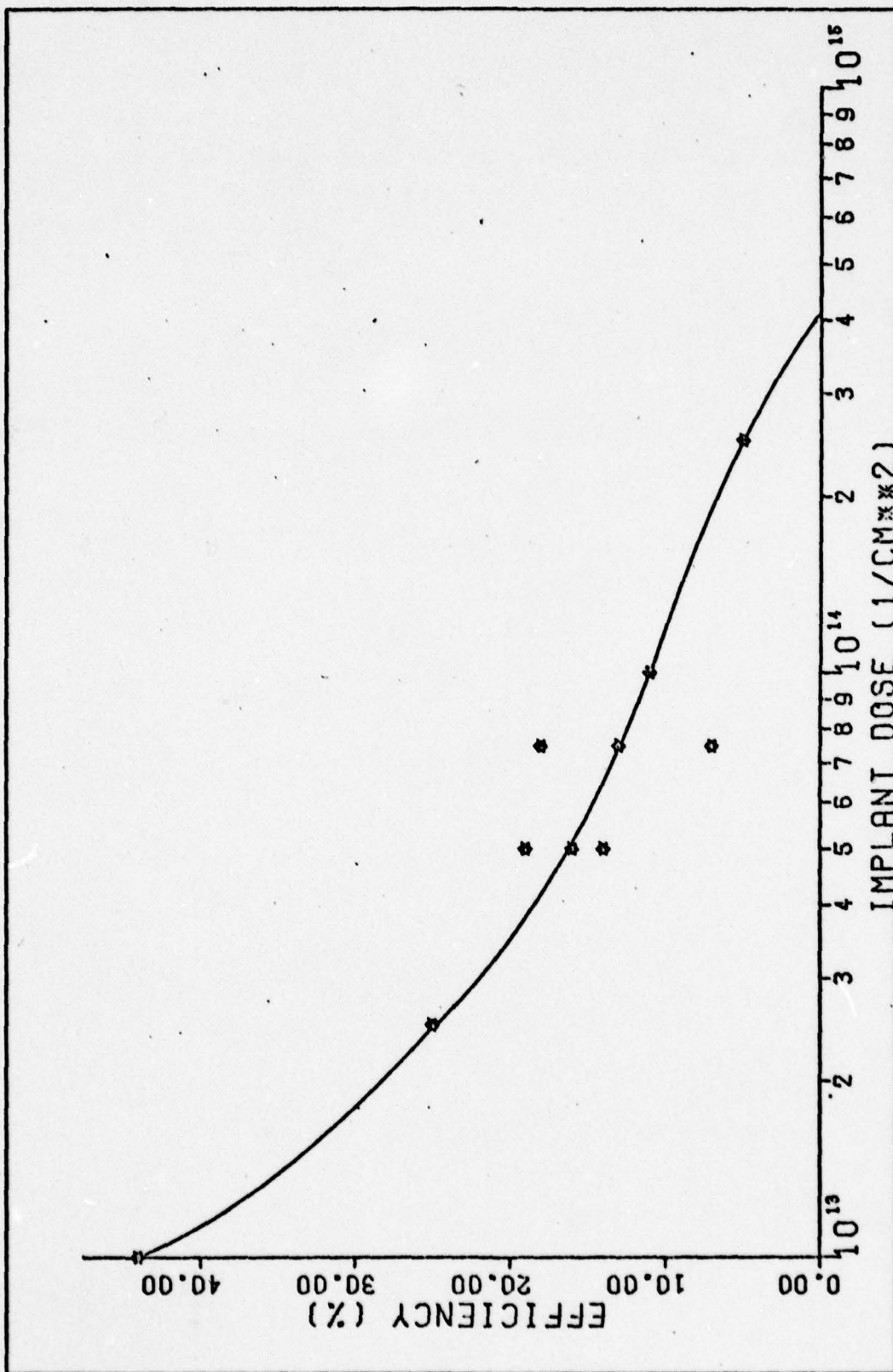


Fig. 39. Percent Type Conversion vs Implant Dose

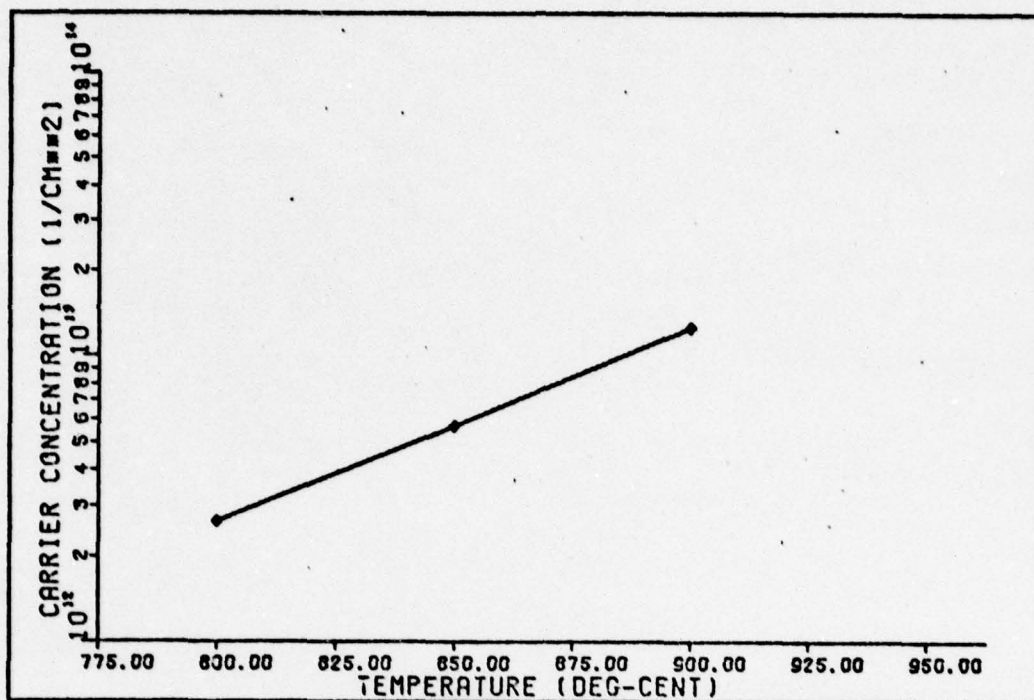


Fig. 40. Carrier Concentration vs Anneal Temperature

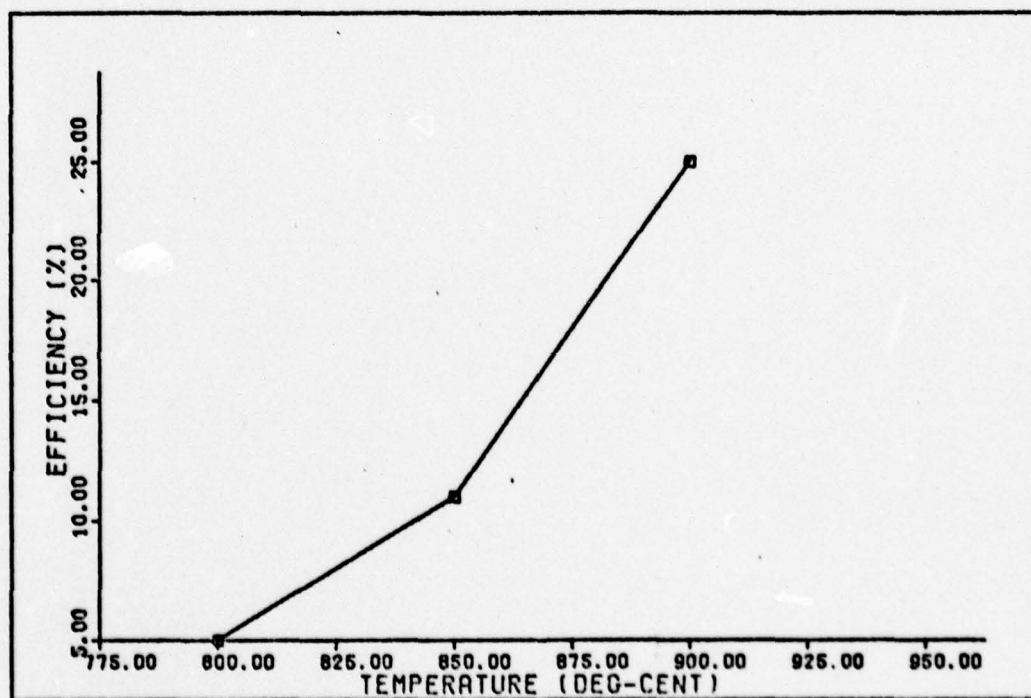


Fig. 41. Efficiency vs Anneal Temperature

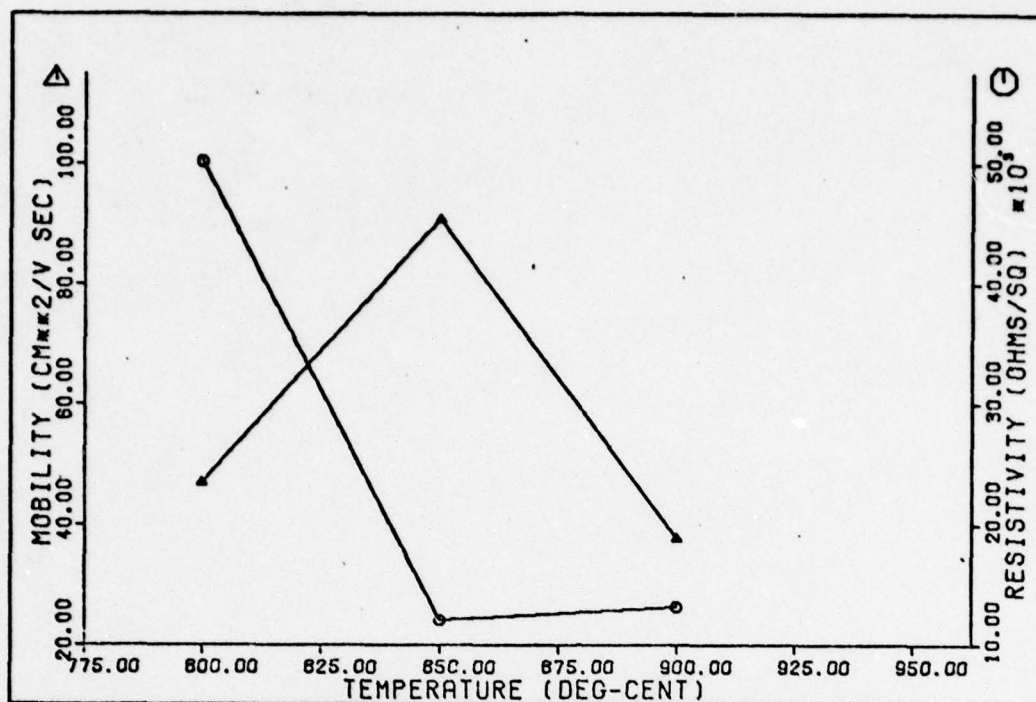


Fig. 42. Mobility and Resistivity vs Anneal Temperature

TABLE II

Anneal Temperature Summary

Anneal Temperature	Implant Dose	Carrier Concentration	Percent Efficiency
800°C	5×10^{13}	2.65×10^{12}	5
850°C	5×10^{13}	5.67×10^{12}	11
900°C	5×10^{13}	1.25×10^{13}	25
950°C	5×10^{13}	*****	**
1000°C	5×10^{13}	*****	**

TABLE III

Caps Summary

Cap Type	Implant Dose	Carrier Concentration	Percent Efficiency
Pyrolytic Si_3N_4	5×10^{13}	1.25×10^{13}	25.0
$\text{Si}_3\text{N}_4/\text{SiO}_2$	5×10^{13}	8.71×10^{12}	17.4
Al_2O_3	5×10^{13}	3.91×10^{12}	7.8
Sputtered Si_3N_4	5×10^{13}	4.22×10^{12}	8.4
Sputtered SiO_2	5×10^{13}	3.79×10^{12}	7.6

IV. Discussion

The magnesium implants as observed in this investigation were not distributed in the substrate as had been expected at the beginning of this study. Based on the results obtained, two explanations have been developed to account for the experimental results. This chapter will discuss the results presented in the previous chapter and will develop the two explanations as to why such results were obtained.

Density Profiles

The LSS theory predicts a Gaussian distribution of the implanted ions within the substrate (Ref 3:22). As can be seen by the profile plots, Figures 9 through 22, this was not what was observed experimentally. Almost all of the profiles show a decreasing concentration with the maximum concentration of the ions located at the surface. The LSS theory predicted that for an implant energy of 129 KeV, as used in this study, the maximum concentration of magnesium ions should have been approximately 1500 Å in from the surface. The theoretical LSS curve is superimposed on the profile plots in Figures 9 and 16.

At first glance, it would seem that the magnesium ions had not been implanted to the depth predicted. However, if this had been the case, there should have been a Gaussian distribution about whatever depth they had been implanted. Since this was not the case, another problem had to exist. For the most part, the profiles appeared as if only the

second half, the decreasing half, of the curve was present. It appeared as if the first 1500 Å of the substrate had been removed. Since no etching had been done between implantation and measurement, this suggested that there might be some other surface-removing action taking place.

Auger analysis had been taken of the caps earlier to determine the best cap to use for annealing. All of the Auger plots showed relatively heavy concentrations of gallium and phosphorus in the caps after annealing. This can be seen in Figures 1a and 1b in Chapter II. The possibility existed that the surface was breaking down and the gallium and phosphorus were diffusing out through the cap during the annealing. Magnesium was probably diffusing out also but the concentration was too small to observe. If the GaP was breaking down, there would have been an effective etching of the surface shifting the resulting surface inward. Together with some out-diffusion of the magnesium, this might have accounted for the low type conversion and the profiles obtained.

Initially, annealing had been discarded as the primary cause of the shifted profiles since out-diffusion would have been matched by inward diffusion resulting in little or no change of the peak. Previous work had suggested that the out-diffusion of the magnesium was the reason for the low type conversion (Ref 2). From the profile plots obtained with this investigation, this would appear not to be the primary reason for the low efficiency.

The combination of the breakdown of the GaP and the out-diffusion of the magnesium might very well have been part of the problem but it was unlikely to have been the entire reason. The shifted amount, 1500 Å, would have been too large an amount to have been removed this way. The Auger plots did not show enough gallium and phosphorus to indicate that this had been happening to this degree.

The Glow Discharge Optical Spectroscopy profile done on an unannealed sample of magnesium implanted GaP supported the idea that the surface was not being removed. Three GDOS profiles were run on annealed and unannealed samples. The profile run on a low resistivity (3.9 Ω) sample indicated that the peak of the concentration distribution was only approximately 75 Å in from the surface. Another profile taken of the high resistivity sample, like those used throughout this investigation, indicated the peak to be exactly at the surface (See Figures 23 and 24). Both of these profiles had been taken of unannealed samples. A GDOS profile of an annealed sample showed the same type of distribution.

The electrical profiles could not have determined if there had been a peak 75 Å in from the surface due to the etch steps experienced. The smallest etch step obtained was greater than 200 Å. Whether or not the peak was at 75 Å or at the surface did not matter, it was still far from the LSS predicted 1500 Å.

Another possible explanation for the profiles observed is based on a theory presented by L. N. Large and R. W.

Bicknel of the Services Electronic Research Laboratory, U. K. (Ref 9). High-energy ions lose their energy as they pass through a solid by collisions with both target electrons and atoms. Bohr's work showed that the most important criterion determining which process was dominant is the velocity of the ions. For particles of high velocity compared with the velocity of the electron in the Bohr model of the hydrogen atom, the dominant energy-loss process is the one in which energy is imparted to the target electrons (the electronic collision process). As the velocity is reduced, the dominant process becomes the one in which energy is imparted to the individual target atoms (the nuclear collision process). When electronic processes dominate in the energy-loss mechanism, the resulting distribution of the implanted ions is as shown in Figure 43. When nuclear collision processes dominate, the resulting distribution is as shown in Figure 44. The profiles obtained experimentally were much the same as this latter type.

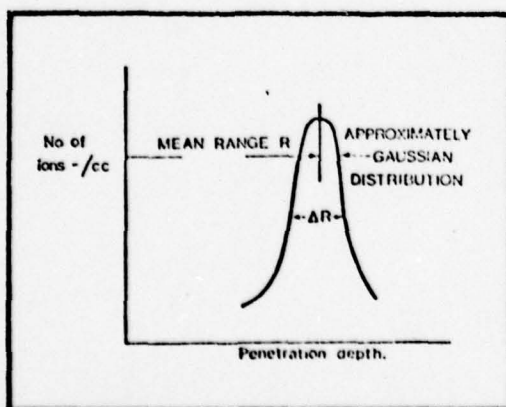


Fig. 43. Distribution of ions when electronic collisions dominate (Ref 9:590)

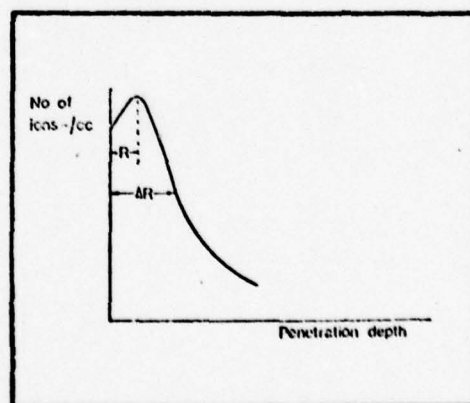


Fig. 44. Distribution of ions when nuclear collisions dominate (Ref 9:590)

The LSS theory is not contradictory to this theory. The LSS theory merely adds both collision processes together. Large indicates that one process might dominate over the other. For low velocity ions, the nuclear process would predominate. Since only 129 KeV was used for this investigation, it is very likely that the magnesium ions used here were of the velocity that caused nuclear collisions to dominate.

Of the two explanations presented, this latter one would appear to be more likely. It is highly unlikely, from the data obtained, that as much as 1500 Å was being removed by the breakdown of the GaP. Both the GDOS profiles and the electrical profiles indicated that the theory presented by Large and Bicknel is correct.

Conversion Efficiency

In all cases, p-type conversion was obtained. The efficiency ranged from as high as 44% to a low of 5%. The average was approximately 17%. The low dose implants gave the highest efficiency. This appeared odd at first but it could be explained by the implant damage associated with the increasing implant doses. Samples implanted with a dose of 10^{15} ions/cm² were so damaged that very little of the damage could be corrected by annealing. The resistivity of these heavily implanted samples was so high that electrical measurements could not be made. The heavy dose had turned the material almost completely amorphous. These results were consistent with those obtained by Gelpey at M.I.T. (Ref 2).

Figure 39 shows how efficiency varied with the implant dose.

Annealing Temperature

All of the profile runs were made using an annealing temperature of 900°C. This temperature was based on work done previously by Inada and Ohnuki, and Gelpey. To verify that this was the most efficient annealing temperature to use, samples were implanted with the same dose (5×10^{13} ions/cm²) and annealed at 800°C, 850°C, 900°C, 950°C, and 1000°C. The results of these tests can be seen in Figures 40 and 41 and Table II. The number of active carriers and thus the percent of efficiency or type conversion increased up to the 900°C run. Samples annealed at 950°C and 1000°C developed severe fractures in the surface due to the high heat. These fractures caused these samples to exhibit extremely high resistivity, thus preventing any Hall measurements. As can be seen in Figure 42, the resistivity of the implanted material decreased as the temperature was increased up to the 900°C limit. This would indicate that more carriers were present. From these results, it appeared that 900°C had been the best temperature to use for annealing.

Caps

Several previous studies had suggested that out-diffusion of the implant was the prime reason for the low efficiency and that a suitable cap would prevent this. To check this theory, several different caps were tried. Sputtered SiO₂, Si₃N₄, and Al₂O₃ and a pyrolytically deposited cap of Si₃N₄

covered by a layer of SiO_2 were the caps tried. The results of these tests are shown in Table III. All but the layered Si_3N_4 and SiO_2 showed efficiencies much less than with the standard pyrolytic Si_3N_4 cap used throughout this investigation. The layered cap was better than the two sputtered caps but was still not as good as the pyrolytic Si_3N_4 . The Si_3N_4 cap showed a higher efficiency here than with the previous profile measurements but was still within the same range. There may be other caps that might give a higher efficiency but these were all that could be obtained for this investigation. However, with the other results obtained with the profiling, the cap would not appear to be the prime reason for low efficiency.

Other Results

Other graphs in Chapter III show that resistivity increased as the depth increased. This was consistent with the decreasing concentration profiles obtained. If there were fewer carriers, the resistance naturally had to be higher. The mobility also increased as depth increased but in a few cases dropped at the last measurement. This drop would indicate that the implanted region had been etched through leaving only the substrate.

Another characteristic was observed that caused concern but proved not to be a significant problem. It was observed that the Si_3N_4 cap caused a slight p-type layer to form during the annealing. Un-implanted samples were measured and it was found that the layer of conversion was less than

100 Å. This p-type layer was probably caused by the GaP breaking down. Gallium has a higher diffusion rate through the cap than phosphorus and would tend to leave a layer of gallium vacancies. This would have caused a p-type layer to be formed. Since the depth of this layer and the percent of conversion was very low, it had little effect on the overall results of this investigation. It would, however, have accounted for the slightly higher surface concentrations observed in some of the profiles.

V. Conclusion

It has been shown that the concentration distribution of magnesium implanted GaP does not follow the normal LSS predicted distribution. The general trend for all samples tested was a decreasing concentration as depth increased. These results agreed with the theory presented by L. N. Large and R. W. Bicknel where nuclear collision processes dominate. In all cases, p-type conversion was obtained with the magnesium implants. The efficiency obtained with this investigation was generally higher than that previously observed by Gelpey and others. An annealing temperature of 900°C was found to be the most efficient and was used throughout this investigation. This agreed with work done by Inada and Ohnui but slightly disagreed with Gelpey's work. This disagreement could be entirely due to different temperature measuring equipment. It is possible that a different annealing cap might give a higher efficiency but from results obtained, Si₃N₄ deposited pyrolytically appeared the best.

One possible method to improve efficiency would be to implant at elevated temperatures thus allowing lower annealing temperatures. More work is needed in this area to determine if this is indeed a feasible method. Other implants should be profiled in GaP to determine if the same type of carrier distribution is obtained as with magnesium. A higher implant energy, above 300 KeV, should be tried to see if a higher energy would cause electronic collision processes to take over and give a Gaussian distribution. A more controlled

etch rate should be used with smaller etch steps to determine if there is a peak in the profile near the surface but not exactly at it. And, of course, this investigation should be repeated to determine the repeatability of the results obtained.

Gallium phosphide has many potential uses due to the wide bandgap and visible light spectrum it possesses. Thus, with more progress in this area, it can become a very useful and important semiconductor material.

Bibliography

1. Dobbs, Bill C., David J. Lank, and Y. S. Park. "Ohmic Contacts on Ion Implanted Gallium Phosphide," Submitted for Publication, Air Force Avionics Laboratory, Wright-Patterson Air Force Base, Ohio, April 1977.
2. Gelpey, Jeffrey C. Electrical Activity of Ion Implanted Impurities in Gallium Phosphide. Masters Thesis. Massachusetts Institute of Technology, Massachusetts, June 1976.
3. Gibbons, James F., et al. Projected Range Statistics. Stroudsburg: Dowden, Hutchinson and Ross, Inc.
4. Hemenger, Patrick M. "Measurement of High Resistivity Semiconductors Using the van der Pauw Method," Review of Scientific Instrumentation 44:698-700 (June 1973).
5. Hemenger, P. M. and B. C. Dobbs. "Zinc ion implantation of sulfur-doped GaP," Applied Physics Letters 23:462-464 (October 1973).
6. Inada, T. and Y. Ohnuki. "Ion Implantations of Mg and Zn into n-type GaP," 4th International Conference on Ion Implantation in Semiconductors and Other Materials, Osaka, Japan (1974).
7. Inada, T. and Y. Ohnuki. "Magnesium and zinc ion implantation into sulfur doped GaP," Applied Physics Letters 25:228-230 (August 1974).
8. Johansson, N. G. E., et al. "Technique Used in Hall Effect Analysis of Ion Implanted Si and Ge," Solid-State Electronics 13:317-335 (1970).
9. Large, L. N. and R. W. Bicknel. "Ion-Implantation Doping of Semiconductors," Journal of Materials Science 2:589-609 (1967).
10. Petersen, P. E., et al. Advanced Development on Gallium Phosphide Materials for Satellite Attitude Sensors. Interim Technical Report. Bloomington, Minnesota, Honeywell Corporation, January 1976.
11. Tomkiewicz, M. and J. M. Woodall. "Photo-Assisted Electrolysis of Water With GaP Electrodes," IBM Technical Bulletin 19:2268 (1976).
12. van der Pauw, L. J. "A Method of Measuring the Resistivity and Hall Coefficient on Lamellae of Arbitrary Shape," Philips Technical Review 20:220-224 (1958-59).

Appendix A

Computer Program to Calculate and Plot Carrier Density, Mobility, and Resistivity

```
PROGRAM HALL(INPUT,OUTPUT,PLOT)
INTEGER X,Y
REAL N(15), MU(15)
DIMENSION R(15),ANGS(15),RHO(15),ANG(15)
REAL NS,I1,I2,I3,I4,I5,I6,I,IA
PHI=3.141592654
E=1.6E-19
A=.693147181
CALL DATE(DAYS)
CALL TIME(HOURS)
PRINT*,"      THIS RUN USES MARSH'S EQUATIONS"
PRINT*,"      THIS DATA IS FOR SAMPLE S-1"
PRINT*
PRINT 877,DAYS,HOURS
J=0
NS=0
ANGS1=0
READ*,B,T
10 CONTINUE
J=J+1
READ*,ANGS(J)
IF(EOF(5LINPUT).NE.0.0)GO TO 40
READ*,I1,I2,I3,I4
READ*,V1,V2,V3,V4,V5,V6,V7,V8
RA=ABS(V1/I1)
RB=ABS(V2/I1)
RC=ABS(V3/I2)
RD=ABS(V4/I2)
RE=ABS(V5/I3)
RF=ABS(V6/I3)
RG=ABS(V7/I4)
RH=ABS(V8/I4)
RAVG=(RA+RB+RC+RD+RE+RF+RG+RH)/8.0
RHO(J)=PHI*RAVG/A
READ*,IA
I=ABS(IA)
PRINT*
READ*,VA1,VA2,VB1,VB2,VC1,VC2,VD1,VD2
READ*,VE1,VE2,VF1,VF2,VG1,VG2,VH1,VH2
VA=ABS(VA1-VA2)
VB=ABS(VB1-VB2)
VC=ABS(VC1-VC2)
VD=ABS(VD1-VD2)
```

```

VE=ABS(VE1-VE2)
VF=ABS(VF1-VF2)
VG=ABS(VG1-VG2)
VH=ABS(VH1-VH2)
R1=VA/I
R2=VB/I
R3=VC/I
R4=VD/I
R5=VE/I
R6=VF/I
R7=VG/I
R8=VH/I
DELTAR=(R1+R2+R3+R4+R5+R6+R7+R8)/8
R(J)=1.0E+08*(DELTAR/B)
GO TO 25
40 CONTINUE
Y=J-1
X=J-2
DO 30 M=1,X
C=(R(M)/(RHO(M)**2))-(R(M+1)/(RHO(M+1)**2))
D=(1.0/RHO(M))-(1.0/RHO(M+1))
IF (R(M).NE.R(M+1))GO TO 33
C=1.0E-99
PRINT*,"MU(",M,") AND N(",M,") INVALID"
33 IF (RHO(M).NE,RHO(M+1)) GO TO 35
D=1.0E-99
PRINT*,"MU(",M,") AND N(",M,") INVALID"
35 MU(M)=ABS(C/D)
N(M)=ABS(D/(E*MU(M)*ANGS(M+1)*1.0E-08))
NS=NS+(N(M)*ANGS(M+1)*1.0E-08)
30 CONTINUE
100 FORMAT(1X,"SWPOS",8X,"I",13X,"V",13X,"R")
150 FORMAT(3X,I1,4X,E11.5,3X,E11.5,3X,E11.5)
200 FORMAT(3X,"FOR A DEPTH OF",F6.0,"ANGSTROMS, THE DATA IS:")
250 FORMAT(18X,"I = ",E11.5)
300 FORMAT(1X,"SWPOS",7X,"V1",12X,"V2",10X,"DELTA R")
350 FORMAT(2X,I2,4X,E11.5,3X,E11.5,3X,E11.5)
400 FORMAL(5X,"SHEET RESISTIVITY(RHO) =",E11.5,1X)
450 FORMAT(5X,"SHEET HALL COEFF =",E11.5)
500 FORMAT(5X,"TOTAL CARRIER DENSITY(N)=",E11.5,1X,"1/CM**2")
550 FORMAT(30X,"AVERAGE R = ",E11.5)
600 FORMAT(24X,"AVERAGE DELTA R = ",E11.5)
650 FORMAT(4X,"DEPTH",4X,"CARRIER DENSITY",4X,"MOBILITY",
10X,"RHO")
700 FORMAT(4X,F5.0,6X,E11.5,4X,E11.5,4X,E11.5)
750 FORMAT(19X,"SUMMARY OF RESULTS")
GO TO 90
25 PRINT 200,ANGS1+NAGS(J)
PRINT*
PRINT*
PRINT 100
PRINT 150,6,I1,V1,RA
PRINT 150,6,I1,V2,RB

```

```

PRINT 150,7,I2,V3,RC
PRINT 150,7,I2,V4,RD
PRINT 150,8,I3,V5,RE
PRINT 150,8,I3,V6,RF
PRINT 150,9,I4,V7,RG
PRINT 150,9,I4,V8,RH
PRINT*
PRINT 550,RAVG
PRINT*
PRINT*
PRINT 250,I
PRINT 300
PRINT 350,10,VA1,VA2,R1
PRINT 350,10,VB1,VB2,R2
PRINT 350,10,VC1,VC2,R3
PRINT 350,10,VD1,VD2,R4
PRINT 350,11,VE1,VE2,R5
PRINT 350,11,VF1,VF2,R6
PRINT 350,11,VG1,VG2,R7
PRINT 350,11,VH1,VH2,R8
PRINT*
PRINT 600,DELTAR
PRINT*
PRINT*
PRINT 400,RHO(J)
PRINT*
PRINT 450,R(J)
PRINT*
PRINT*
ANGS1=ANGS1+ANGS(J)
ANG(J)=ANGS1
GO TO 10
90 CONTINUE
PRINT 750
PRINT*
PRINT 650
PRINT*, "*****"
DO 20 K=1,X
PRINT 700,ANG(K),N(K),MU(K),RHO(K)
20 CONTINUE
PRINT*
PRINT 500,NS
PRINT*
PRINT 877,DAYS,HOURS
877 FORMAT(8X,"DATE OF THIS RUN   ",A10,10X,"TIME   ",A10)
CALL PLOT(0.0,-11.0,-3)
CALL PLOT(1.0,2.0,-3)
CALL SCALE(ANG,7.5,X,1)
CALL LGSCAL(N,4.75,X)
CALL LGAXIS(0.0,0.0,25HCARRIER DENSITY (1/CM**3),25,
&4.75,90.,N(X+1),N(X+2))
CALL AXIS(0.,0.,17HDEPTH (ANGSTROMS),-17,7.5,0.,
&ANG(X+1),ANG(X+2))

```



```

CALL LGLINE(ANG,N,X,1,1,1)
CALL SYMBOL(1.0,4.75,0.21,3)OHELECTRICAL PROFILE OF CHIP
&S-1,0.,30)
CALL RECT(-.75,-.5,5.75,8.75,0.0,3)
CALL RECT(-1.875,-2.0,8.5,11.0,0.0,3)
CALL PLOT(11.0,-10,-3)
CALL PLOT(1.0,2.0,-3)
CALL SCALE(MU,4,75,X,1)
CALL SCALE(RHO,4.75,X,1)
CALL AXIS(0.,0.,22HMOBILITY (CM**2/V SEC),22,4.75,90.,
&MU(X+1),MU(X+2))
CALL AXIS(7.5,0.,21HRESISTIVITY (OHMS/SQ),-21,4.74,90.,
&RHO(X+1),RHO(X+2))
CALL AXIS(0.,0.,17HDEPTH (ANGSTROMS),-17,7.5,0.,
&ANG(X+1),ANG(X+2))
CALL LINE(ANG,MU,X,1,1,2)
CALL LINE(ANG,RHO,X,1,1,1)
CALL SYMBOL(-.25,4.7,.21,2,0.,-1)
CALL SYMBOL(7.75,4.7,.21,1,0.,-1)
CALL RECT(-.625,-.5,5.75,8.75,0.0,3)
CALL RECT(-1.875,-2.0,8.5,11.0,0.0,3)
CALL PLOTE
STOP
END

```

Appendix B

The Lindhard, Scharff, and Schiott Theory

The LSS theory describes the distribution of implanted atoms in an amorphous solid. In application to semiconductor material, the amorphous solid is approximated by implanting along an axis which is not parallel to any channels in the lattice. In this thesis, the implants were made approximately 7° off the [111] direction. The LSS theory considers the stopping power of the atoms in the substrate on the implanted ions through a kinetic energy loss argument. The result is a Gaussian distribution in which the range, R_p , (position of the peak of the distribution) and the standard deviation, ΔR_p , depend on the implant energy and the atomic numbers of the implanted ion and the substrate material. Gibbons and Johnson have developed a computer program to calculate R_p and ΔR_p and tabulate the results for various energies, substrates, and implanted ions (Ref 3).

The concentration, $N(x)$, of the implanted ions from the substrate surface is obtained by:

$$N(x) = \frac{\phi}{\Delta R_p \sqrt{2\pi}} \exp \left[-\frac{(x-R_p)^2}{2\Delta R_p^2} \right] \quad (B1)$$

where x is measured along the direction of incidence of the beam and

ϕ = fluence, or ion dose/cm²

ΔR_p = standard deviation in projected range

R_p = projected range

The R_p and ΔR_p can be obtained from Gibbons and Johnson's computer listings such as is in Appendix C.

The resulting doping profile will be similar to the theoretical distribution shown in Figure B1. Low energy implants result in profiles with the peak closer to the surface. When used for p - n junctions, the junction depth is at the point where the profile crosses the background impurity level.

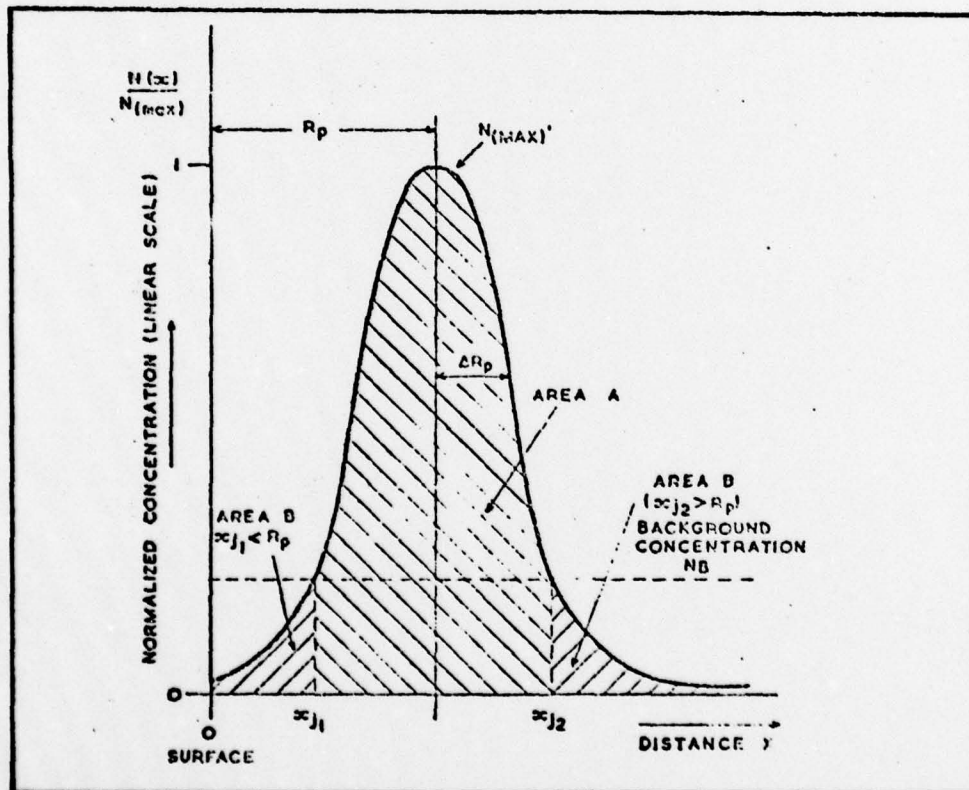


Fig. B1. Typical Theoretical Gaussian Ion Distribution
(Ref 2:79)

LESS RANGE STATISTICS FOR MAGNESIUM									
IN GALLIUM	PHOSPHOR	ENERGY (KEV)	RANGE (MICRONS)	STANDARD DEVIATION	RANGE (MICRONS)	DEFINITION	NUCLEAR LOSS	ELECTRONIC LOSS	ENERGY LOSS
SUBSTRATE PARAMETERS-									
		10	.0122	.0077	.0222	.0077	.0077	.0077	.0077
		20	.0245	.0152	.0440	.0152	.0152	.0152	.0152
		30	.0368	.0213	.0660	.0213	.0213	.0213	.0213
		40	.0491	.0273	.0979	.0273	.0273	.0273	.0273
		50	.0614	.0333	.1298	.0333	.0333	.0333	.0333
		60	.0737	.0393	.1617	.0393	.0393	.0393	.0393
		70	.0860	.0453	.1936	.0453	.0453	.0453	.0453
		80	.0983	.0513	.2255	.0513	.0513	.0513	.0513
		90	.1106	.0573	.2574	.0573	.0573	.0573	.0573
		100	.1229	.0633	.2893	.0633	.0633	.0633	.0633
		110	.1352	.0693	.3212	.0693	.0693	.0693	.0693
		120	.1475	.0753	.3531	.0753	.0753	.0753	.0753
		130	.1598	.0813	.3850	.0813	.0813	.0813	.0813
		140	.1721	.0873	.4169	.0873	.0873	.0873	.0873
		150	.1844	.0933	.4488	.0933	.0933	.0933	.0933
		160	.1967	.0993	.4807	.0993	.0993	.0993	.0993
		170	.2090	.1053	.5126	.1053	.1053	.1053	.1053
		180	.2213	.1113	.5445	.1113	.1113	.1113	.1113
		190	.2336	.1173	.5764	.1173	.1173	.1173	.1173
		200	.2459	.1233	.6083	.1233	.1233	.1233	.1233
		210	.2582	.1293	.6402	.1293	.1293	.1293	.1293
		220	.2705	.1353	.6721	.1353	.1353	.1353	.1353
		230	.2828	.1413	.7040	.1413	.1413	.1413	.1413
		240	.2951	.1473	.7359	.1473	.1473	.1473	.1473
		250	.3074	.1533	.7678	.1533	.1533	.1533	.1533
		260	.3197	.1593	.7997	.1593	.1593	.1593	.1593
		270	.3320	.1653	.8316	.1653	.1653	.1653	.1653
		280	.3443	.1713	.8635	.1713	.1713	.1713	.1713
		290	.3566	.1773	.8954	.1773	.1773	.1773	.1773
		300	.3689	.1833	.9273	.1833	.1833	.1833	.1833
		310	.3812	.1893	.9592	.1893	.1893	.1893	.1893
		320	.3935	.1953	.9911	.1953	.1953	.1953	.1953
		330	.4058	.2013	.1020	.2013	.2013	.2013	.2013
		340	.4181	.2073	.1079	.2073	.2073	.2073	.2073
		350	.4304	.2133	.1138	.2133	.2133	.2133	.2133
		360	.4427	.2193	.1197	.2193	.2193	.2193	.2193
		370	.4550	.2253	.1256	.2253	.2253	.2253	.2253
		380	.4673	.2313	.1315	.2313	.2313	.2313	.2313
		390	.4796	.2373	.1374	.2373	.2373	.2373	.2373
		400	.4919	.2433	.1433	.2433	.2433	.2433	.2433
		410	.5042	.2493	.1492	.2493	.2493	.2493	.2493

Fig. C1. Gibbons and Johnson Range Estimates Listing for Mg Implanted GaP


VITA

David James Lank was born on 21 April 1949 in Salisbury, Maryland. He graduated from high school in Salisbury in 1967 and entered Clemson University from which he received the degree of Bachelor of Science in Electrical and Computer Engineering in May 1971. Upon graduation, he was commissioned in the USAF through the ROTC program. He immediately began active duty and attended Missile Officer School where he certified as a Deputy Missile Combat Crew Commander. He then served as Deputy Missile Combat Crew Commander, Missile Combat Crew Commander, Instructor, and Missiles Procedures Trainer Operator with the 44th Strategic Missile Wing, Ellsworth AFB, South Dakota until May 1976. He then served a short period of time with the 6595th Space Test Group, Vandenberg AFB, California as Chief, Electrical Systems Branch, Scout Division until entering the School of Engineering, Air Force Institute of Technology, in August 1976.

Permanent address: Rapid City, South Dakota
57701

UNCLASSIFIED

SECURITY CLASSIFICATION OF THIS PAGE (When Data Entered)

REPORT DOCUMENTATION PAGE		READ INSTRUCTIONS BEFORE COMPLETING FORM
1. REPORT NUMBER AFIT/GE/EE/77-38	2. GOVT ACCESSION NO.	3. RECIPIENT'S CATALOG NUMBER
4. TITLE (and Subtitle) ELECTRICAL PROFILING OF MAGNESIUM IMPLANTED GALLIUM PHOSPHIDE		5. TYPE OF REPORT & PERIOD COVERED MS Thesis
7. AUTHOR(s) David J. Lank Capt USAF		6. PERFORMING ORG. REPORT NUMBER
9. PERFORMING ORGANIZATION NAME AND ADDRESS Air Force Institute of Technology (AFIT-EN) Wright-Patterson AFB, Ohio 45433		8. CONTRACT OR GRANT NUMBER(s)
11. CONTROLLING OFFICE NAME AND ADDRESS Air Force Avionics Laboratory (DHR) Wright-Patterson AFB, Ohio 45433		10. PROGRAM ELEMENT, PROJECT, TASK AREA & WORK UNIT NUMBERS
14. MONITORING AGENCY NAME & ADDRESS (if different from Controlling Office)		12. REPORT DATE December 1977
		13. NUMBER OF PAGES 79
		15. SECURITY CLASS. (of this report) Unclassified
		15a. DECLASSIFICATION/DOWNGRADING SCHEDULE
16. DISTRIBUTION STATEMENT (of this Report) Approved for public release; distribution unlimited.		
17. DISTRIBUTION STATEMENT (of the abstract entered in Block 20, if different from Report)		
18. SUPPLEMENTARY NOTES Approved for public release; IAW AFR 190-17  JERRAL F. GUESS, Captain, USAF Director of Information		
19. KEY WORDS (Continue on reverse side if necessary and identify by block number) Gallium Phosphide Differential Hall Profiling Electrical Profiling van der Pauw Method Magnesium Implanted GaP Ion Implantation GDOS		
20. ABSTRACT (Continue on reverse side if necessary and identify by block number) Differential Hall measurements by the van der Pauw technique were taken to provide a profile of the electrically active carriers in ion implanted GaP. The study was limited to magnesium implants at room temperature. The profiles indicated a decreasing carrier density as depth increased. The peak of the profiles was at or near the surface. GDOS profiles taken of the samples indicated the same type of profile. The LSS theory did not appear to hold true in this study. Temperature and cap dependence runs were also done.		